# STATIC STABILITY AND COMBUSTION FEATURES OF $C_3H_8/O_2/CO_2$, $C_3H_8/O_2/N_2$ AND $CH_4/H_2/O_2/CO_2$ TURBULENT PREMIXED FLAMES IN A MODEL GAS TURBINE COMBUSTOR


BY

**ASIF ALI**


A Thesis Presented to the

DEANSHIP OF GRADUATE STUDIES

**KING FAHD UNIVERSITY OF PETROLEUM & MINERALS**

DHAHRAN, SAUDI ARABIA

In Partial Fulfillment of the
Requirements for the Degree of

**MASTER OF SCIENCE**

In

**MECHANICAL ENGINEERING**

**MARCH 2020**

KING FAHD UNIVERSITY OF PETROLEUM & MINERALS

DHAHRAN- 31261, SAUDI ARABIA

**DEANSHIP OF GRADUATE STUDIES**

This thesis, written by Asif Ali under the direction of his thesis advisor and approved by his thesis committee, has been presented and accepted by the Dean of Graduate Studies, in partial fulfillment of the requirements for the degree of MASTER OF SCIENCE IN MECHANICAL ENGINEERING.

Dr. Muhammad Mustafa Kamal
(Advisor)

Zuhair Gasem

Dr. Zuhair Mattoug Gasem
Department Chairman

Dr. Mohammad Abdulaziz Mustafa Habib
(Co-Advisor)

Dr. Salam A. Zummo
Dean of Graduate Studies

Syed Said

Dr. Syed Ahmad Mohammad Said
(Member)

23-4-2020
Date

Dr. Ahmet Sakin
(Member)

Dr. Medhat Ahmed Nemitallah
(Member)

I would like to dedicate my thesis work to my beloved parents and teachers.

# ACKNOWLEDGMENTS

I would like to express my gratitude to the KFUPM for giving me this opportunity to avail fully funded Master of Science scholarship program in Mechanical Engineering.

It would be my pleasure to thank my advisor Dr. Muhammad Mustafa Kamal for his valuable supervision throughout my thesis. He has always accommodated me for discussing thesis related issues and has provided with simple yet effective suggestions. Along with consistent guidance, he inspired me during the course of this thesis. He has specifically taught me skills to carry out effective literature review and the analysis of results obtained from our research. He also offered several plausible suggestions, based on his precious experience, for the future prospects related to my career.

I am indebtedly thankful to my co-advisor Dr. Mohammed Abdulaziz Mustafa Habib for continuous support during my thesis. I would also like to thank my committee members Dr. Syed Ahmad Mohammad Said, Dr. Ahmet Sahin and Dr. Medhat Ahmed Nemitallah for adding value to my thesis with their valuable suggestions. Especially, Dr. Medhat guided me all the way in the numerical research. It would be my pleasure to mention my gratitude towards Dr. Ahmed Abdelhafez for enriching my thesis especially for providing his valuable insight on data analysis and experimental techniques. I would like to express my gratitude towards my friends, colleagues, seniors and lab attendants for making this thesis work possible for me.

I would also like to thank my family for helping me throughout my life. I have completed my graduate studies because of their consistent love and support.

# TABLE OF CONTENTS

# LIST OF FIGURES

# LIST OF ABBREVIATIONS

| | |
|---|---|
| $A$ | Burner throat cross-sectional area [$m^2$] |
| *AFT* | Adiabatic flame temperature [K] |
| $CO_2$ | Carbon dioxide |
| $CH_4$ | Methane |
| $D$ | Diameter of the burner throat [m] |
| DLE | Dry low emission |
| $H_2O$ | Water vapor |
| LPM | Lean premixed |
| $\dot{m}$ | Mass flow rate [kg/s] |
| $M$ | Molecular weight [kg/mole] |
| $N_2$ | Nitrogen |
| $O_2$ | Oxygen |
| OEC | Oxygen-enhanced combustion |
| *OF* | Oxygen fraction; volumetric fraction of $O_2$ in $O_2$/X diluted oxidizer |
| $p$ | Pressure in combustor [kPa] |
| *PD* | Power density of combustor [$MW/m^3/bar$] |
| $R_u$ | Universal gas constant [kJ/kmol/K] |
| *Re* | Reynolds number at combustor throat |
| $T$ | Absolute reactant temperature [K] |
| $v$ | Bulk throat velocity [m/s] |
| $v_a$ | Bulk throat velocity axial component [m/s] |
| X | Diluent gas, either $CO_2$ or $N_2$ |
| $y$ | Mole fraction |
| LES | Large eddy simulation |
| *HF* | Hydrogen fraction |
| $U_{in}$ | Inlet bulk velocity |

*ORZ* Outer recirculation zone

*SE* Secondary eddy

*IRZ* Inner recirculation zone

*PE* Primary eddy

*Re* Reynolds number

*Da* Damköhler number

*TFS* Turbulent flame speed [m/s]

*LFS* Laminar flame speed [m/s]

*DO* Discrete ordinate

*LBO* Lean blowout

*Ls* Mixing length scale [m]

*Sw* Swirl number

$f$ Mixture fraction

$u'$ Root mean squared turbulent fluctuations [m/s]

$f'$ Mixture fraction variance

Greek symbols

$\varphi$ Equivalence ratio

$\rho$ Density [kg/m$^3$]

$\mu$ Dynamic viscosity [kg/m/s]

$\alpha$ Thermal diffusivity [m$^2$/s]

$\delta$ Flame thickness [m]

$\lambda$ Thermal conductivity [W/m K]

$\Gamma_\varphi$ Diffusion coefficient [m$^2$/s]

$k$ Turbulent kinetic energy [m$^2$/s$^2$]

$\nu$ Kinematic viscosity [$m^2/s$]

$\varepsilon$ Turbulent dissipation rate [$m^2/s^3$]

$\eta$ Efficiency

$\mu_t$ Turbulence viscosity [kg/m s]

$\tau_{ij}$ Subgrid-scale stress tensor [$N/m^2$]

Subscripts

mix Reactant mixture ($C_3H_8 + O_2 + X$)

$i$ Each mixture constituent

# ABSTRACT

Full Name : Asif Ali

Thesis Title : Static stability and combustion features of $C_3H_8/O_2/CO_2$, $C_3H_8/O_2/N_2$ and $CH_4/H_2/O_2/CO_2$ turbulent premixed flames in a model gas turbine combustor

Major Field : Mechanical Engineering

Date of Degree : March 2020

This thesis work aims at investigating and comparing the macrostructure and stabilization modes of swirl-stabilized premixed oxygen-enriched air-propane ($C_3H_8/O_2/N_2$) and oxy-propane ($C_3H_8/O_2/CO_2$) turbulent flames in a model gas turbine combustor, under similar conditions of equivalence ratio ($\varphi$ = 0.1 - 1.0), bulk throat velocity ($U_{in}$) of 5.2 m/s and oxygen fraction (*OF* = 21% - 70%). The constant contours of adiabatic flame temperature (*AFT*) were plotted with combustor stability maps within the $\varphi$-*OF* domain for both $CO_2$ and $N_2$ flames. Nominated flames were captured for studying the effects of *AFT* on flame stability and structure. The radial and axial temperatures were measured inside the quartz confinement for getting an insight of thermal flow field. It was found for both $CO_2$ and $N_2$ flames that the blowout and flashback limits followed constant *AFT* contours on the stability map. Even the $CO_2$ and $N_2$ flames of different *OF* and $\varphi$ represented similar structure at identical *AFT*. While the flames possessing similar *OF* or $\varphi$ (resulting in different *AFT*) exhibited distinct flame macrostructure. This defined the dominance of *AFT* parameter in controlling the flame dynamics. This finding would be handy for gas turbine designers, manufacturers and operators in retrofitting the existing air-based combustors to the reduced-emissions oxy-fuel combustors.

Large Eddy Simulation (LES) work was also carried out for investigating the combustion and emission characteristics of stoichiometric hydrogen-enriched oxy-methane ($CH_4/H_2/O_2/CO_2$) flames. The study focused on the effects of hydrogen fraction (*HF*), oxygen fraction (*OF*) and inlet bulk velocity ($U_{in}$) of the combustible mixture on stability and combustion characteristics of the flames. Constant $U_{in}$ of 4.4 m/s, 5.2 m/s and 6.0 m/s were investigated in this analysis. The results indicated that reaction rates are increased with increasing *HF* and *OF*, resulting in compact flames. The CO emissions increased from 140 ppm at *HF*=20% to 279 ppm at *HF*=60%, and these emissions increased from 140 ppm at *OF*=30% to 594 ppm at *OF*=38%. The Damköhler number *(Da)* increases with increasing *HF* and *OF*, while it showed declining behavior with increasing $U_{in}$ because of smaller residence time. It was found that the physical parameter ($U_{in}$) slightly affects the flame kinetics, as compared to the chemical factors (*HF* and *OF*). It was also noticed that the role of the *OF* is more dominant in contrast to *HF*, and even smaller increments in *OF* significantly affects the flame dynamics. This finding was reasoned with the increased chemical kinetics due to enhanced concentrations of O atoms, which oxidize fuel species and results in efficient combustion. The reaction rates thus dominate the flame behavior, while turbulence affects only the macrostructure of the flame.

# ملخص الرسالة

**الاسم الكامل:**آصف علي

**عنوان الرسالة: الاستقرار السكوني ومميزات الاحتراق للهب المضطرب من نوع $C_3H_8/O_2/CO_2$ و$C_3H_8/O_2/N_2$ و $CH_4/H_2/O_2/CO_2$ الممزوج مسبقاً في غرفة الاحتراق التوربيني الغازي النموذجي**

**التخصص: الهندسة الميكانيكية**

**تاريخ الدرجة العلمية**: آذار 2020

تهدف هذه الرسالة إلى دراسة ومقارنة أوضاع الهيكل الكلي والاستقرار للهب المضطرب المستقر والممزوج مسبقاً من لهب غني بالاكسجين والمحتوي على بروبان هوائي ($C_3H_8/O_2/N_2$) ولهب محتوي على بروبان مؤكسد ($C_3H_8/O_2/CO_2$) في غرفة الاحتراق التوربيني الغازي النموذجي، تحت نفس الظروف لنسبة التكافؤ ($\varphi$ = 0.1 - 1.0)، السرعة الكلية عند المدخل ($U_{in}$) المساوي لـ 5.2 متر/ث، ونسبة محتوى الأكسجين (*OF*=21% - 70%). لقد تم رسم الخطوط الكفافية (الكنتورية) لدرجة حرارة اللهب الأديباتي (*AFT*) بخرائط استقرار غرفة الاحتراق ضمن نطاق ال φ-*OF* لكل من لهب $CO_2$ و $N_2$ . تم رصد كلا النوعين من اللهب لدراسة تأثير ال *AFT* على استقرار وبنية اللهب. لقد تم رصد درجات الحرارة الشعاعية والمحورية داخل وعاء الكوارتز للوصول إلى فهم مجال التدفق الحراري. وُجد أن حدود النفخ والاتجاع لكل من لهب $CO_2$ و $N_2$ قد اتبعت خطوط *AFT* الكنتورية الثابتة على خريطة الاستقرار، على الرغم من أن لهب $CO_2$ و$N_2$ ذوي قيم *OF* و φ مختلفة قد مثّلا بنيتين متماثلتين عند نفس قيم ال *AFT*. في حين أن اللهب الذي يمتلك قيم متساوية من OF او φ (ناتجة من قيم مختلفة من AFT) قد أظهر بنية لهبية متباينة. هذا بدوره قد حدد مقدار تغلب العامل AFT في التحكم بديناميكية اللهب. هذه النتيجة ستكون مفيدة لمصممي التوربينات الغازية والمصنعين والمشغلين العاملين في اعادة تأهيل المحارق القائمة المعتمدة على الهواء لتصبح محارق معتمدة على وقود الاوكسي منخفضة الابنعاثات. بالإضافة إلى ذلك، فقد تم إجراء محاكاة الدوامة الكبيرة (LES) لدراسة خصائص الاحتراق والانبعاث للهب الميثان المؤكسد ($CH_4/H_2/O_2/CO_2$) ذوالمكونات المتكافئة والغني بالأكسجين.ركزت الدراسة على تأثير نسبة الهيدروجين (HF)، نسبة الأكسجين(*OF*)، والسرعة الكلية عند المدخل للمزيج القابل للاشتعال على خصائص استقرار واحتراق اللهب. تم فحص قيم ثابتة من ال $U_{in}$ خلال عملية التحليل على النحو التالي 4.4m/s, 5.2 m/s, 6.0m/s. أشارت النتائج أن سرعات التفاعل قد زادت عند زيادة ال(*HF*) وال(*OF*)، مما نتج عنه نيران مضغوطة. بالإضافة إلى ذلك، فإن انبعاثات ال CO قد زاد تركيزها من 140 ppm عند *HF*=20% إلى 279 ppm عند *HF*=60%، وأن هذه الانبعاثات قد زاد تركيزها من 140 ppm عند *OF*=30% إلى 594 ppm عند *OF*=38%. لقد لوحظ أن رقم دامكولر (Damköhler number - *Da*) يزيد عند زيادة ال *HF* وال *OF*، بينما ينخفض هذا الرقم عند زيادة قيمة ال $U_{in}$ بسبب قصر وقت الركود. وقد وجد أن العامل الفيزيائي (Uin) يؤثر قليلاً على حركية اللهب، مقارنة بالعوامل الكيميائية (HF و OF). ولوحظ أيضًا أن دور OF أكثر هيمنة، على عكس HF ، وحتى الزيادات الصغيرة في OF تؤثر بشكل كبير على ديناميكيات اللهب. يمكن الاستدلال على هذا الاستنتاج من خلال زيادة الحركية الكيميائية بسبب التركيزات المعززة لذرات O ، والتي تؤكسد أنواع الوقود وتؤدي إلى احتراق فعال. من ذلك يمكن الاستنتاج بأن سرعة التفاعلات هي من يحكم سلوك اللهب، بينما تؤثر درجة الاضطراب على المكونات الكلية للهب فقط.

# CHAPTER 1

# INTRODUCTION

With advancement in technology and economy, the global power demand is escalating and requires reliable and environmentally friendly sources of energy. According to the International Energy Agency (IEA) expectations, more than 30% of the global energy demand will be increased by 2040 [1]. Due to the improved power density and efficiency, combustion is responsible for majority of the current energy supply and it is likely to play this significant part in foreseeable future. The swift growth in the demands of energy, fossil fuels reserves depletion and hazardous nature of combustion emissions are demanding researchers to look for reliable and cleaner methods of energy conversion [2,3]. So that the available fossil fuels reserves can be utilized as efficiently and cleanly as they could be.

Air is utilized for combustion of fossil fuels in most of the existing combustion applications including gas turbines. Exhaust of fuel oxidized with air comprises mainly of $CO_2$, $H_2O$, $O_2$, $N_2$, and $NO_x$. Among these exhaust gases; $CO_2$ is a greenhouse gas being the reason of ever rising global warming problem. Presently, global energy mix is heavily relying on the fossil fuels for energy harnessing and is projected to remain for several years to come. While $CO_2$ is a certain product of fossil fuel combustion, with ever increasing stricter regulations on emissions, it becomes necessary to explore ways for its separation and capture. When $CO_2$ is in a mixture with other exhaust products especially NOx, it is both expensive and complicated to separate and capture it [4].

## 1.1 Oxy-fuel Combustion

Oxy-fuel combustion stands out as one of the promising solutions to this problem. When pure $O_2$ is used as an oxidizer instead of air, the main products of fossil fuel combustion are $CO_2$ and $H_2O$. Simple condensation is a cost-economic process, which removes $H_2O$ from exhaust, thereby leaving $CO_2$ ready for capture. Removal of $N_2$, which makes about 79% of air by volume, from the products, causes improvement in the efficiency of treatment equipment, and it also, reduces the size of the hardware. Moreover, the absence of $N_2$ in reactants reduces the probability of molecular interactions of $N_2$ and $O_2$ at elevated temperatures at first, which in turn nearly eliminates the possibility of thermal $NO_x$ formation (via Zeldovich mechanism [5]) in oxy-fuel combustion. Air- and oxygen-based combustion systems, on the opposite way, have significantly varied degrees of freedom, in terms of their stable operation. Air is an abundantly available resource, so it is usually used in higher proportions with the fuel in order to achieve complete combustion in various applications. Lean operation also results in reduced combustion temperatures, thus safeguarding the structural integrity of the combustor. Since pure oxygen is an expensive product in itself, most of the oxy-fuel combustion applications are usually operated at or near stoichiometric conditions. On contrary, in absence of $N_2$ gas that acts as a third body, absorbing the heat of combustion, this stoichiometric operation of oxy-fuel combustion consequently approaches to higher temperatures. Due to this reason, pure $O_2$ is diluted with recycled $CO_2$ by using exhaust gas recirculation (EGR), for reduction of combustion temperature. Oxy-fuel combustion thus, have fuel and $O_2/CO_2$ oxidizer as its reactants. However, since $CO_2$ has greater heat capacity and lower thermal diffusivity and chemical dissociation [3,4] on contrary to $N_2$, the substitute of $N_2$ with $CO_2$ lowers down *LFS* and

combustion temperatures in oxy-fuel combustion in comparison to air-fuel one [5-8]. Due to this reason, 21% $O_2$ in $O_2/CO_2$ oxidizer mixture is not achievable and, therefore, $O_2$ composition should be more than this composition in the oxidizer mixture for achieving stable flames.

## 1.2 Lean Premixed Combustion

Fuel and oxidizer mixtures are thoroughly blended before reaching combustor and resulting flames are termed as premixed flames. When this combustion phenomena proceeds below stoichiometric conditions; the fuel is efficiently utilized, and these flames are termed as lean premixed (LPM) flames. With stricter environmental regulations and depleting reservoirs of fossil fuels, it will be one of the significant motivations for the existing LPM air-based combustion customers to switch towards oxy-fuel combustion without any substantial hardware changes. Understanding the behavior of stable flames is essential for switching in between oxidizers. In addition, different fuels have distinct combustion and emission characteristics, and thereby different combustor stability behaviors. This signifies development of a combustor equipped with fuel-flexibility which can utilize various fuels using premixed oxy-combustion technique.

## 1.3 Oxygen-Enriched Air Combustion

Air, which is about 79% $N_2$ and 21% $O_2$ by volume, is being currently used as an oxidizer for majority of the combustion applications. However, the role of oxidant is chemically played by $O_2$ while $N_2$ behaves as a stability agent for the combustion process. $N_2$ carries heat along with it through exhaust from the combustor, resulting in relatively reduced

temperature and therefore decreased thermal efficiency. Most of the thermal processes use elevated proportions of $O_2$ in air for high temperature applications. Such combustion processes are termed as oxygen-enriched air combustion (OEAC). The $O_2$ enrichment of air-based combustion results in improved flame characteristics, higher heat transfer efficiency, rising processing rates, enhanced product quality and reduced equipment cost [12] but possesses a disadvantage in terms of increased NOx emissions. However, these benefits of OEC can turn upside down if combustion system is improperly designed, as further problems originate and may cause non uniform heating, elevated concentrations of pollutants and even burner or refractory damage.

There are generally four primary ways [12] of enhancing combustion process with oxygen: (1) $O_2$ lancing i.e. adding $O_2$ in air/fuel flame, (2) premix enrichment or low-level $O_2$ enrichment i.e. $O_2$ is injected in the combustor approaching air stream, (3) air-oxy/fuel combustion i.e. burner is provided with air and $O_2$ separately, (4) oxy/fuel combustion i.e. high purity $O_2$ replaces air and it is being considered as a favorable prospect of capturing carbon from the exhaust gases [13–15]. The present study utilizes this third and fourth techniques for investigating and comparing the stability and combustion characteristics of propane-based flames.

Low-level $O_2$ enrichment (21-30% $O_2$) requires little modifications in burner for permitting its operation. The cases, where small amounts of $O_2$ enrichment significantly increases the rate of production of the heating process, utilize this low-level $O_2$ enrichment technique, as it economically saves retrofitting cost of the burner. Existing air/fuel burners require replacement with explicitly designed burners for intermediate (30-90% $O_2$) and high-level (>90% $O_2$) oxygen-enrichment cases.

## 1.4 Oxy-fuel and Air-fuel Combustion - A Comparison

Oxy-fuel combustion results in elevated temperatures reaching to hazardous levels. Unlike air-fuel combustion, oxy-fuel combustion is generally operated under stoichiometric conditions because air is an abundant free of cost resource while burning with pure $O_2$ is a relatively expensive process. It is therefore recommended to dilute $O_2$ with exhaust gas, primarily composing of $CO_2$ and $H_2O$, in oxy-fuel combustion where $H_2O$ could be easily detached with the help of economic condensation process. The use of $CO_2$ gas with $O_2$ as an oxidizer mixture reduces down the combustor temperature. However, while comparing the oxy-fuel combustion to the air-fuel one, the flame characteristics such as mass diffusivity, heat capacity, thermal conductivity and dynamic viscosity are affected with the replacement of $N_2$ with $CO_2$ [16–18]. Reaction rates, combustion efficiency and flame speed are reported to be adversely affected with $CO_2$ presence [19]. The stability and flame characteristics with the $O_2/CO_2$ oxidizer mixture are therefore different as compared to the $O_2/N_2$ ones. The combustion characteristics of propane with $O_2/N_2$ and $O_2/CO_2$ oxidizer mixtures have rarely been investigated. This information will aid the gas turbine designers and operators in development of oxygen-enriched air-propane and oxy-propane gas turbines.

## 1.5 Hydrogen Enriched Combustion

The oxidizer mixture of $O_2$ and $CO_2$ presents unwelcomed instabilities and varied combustion behavior in contrast to air-based combustion, as discussed [8]. It has been reported that increasing concentrations of $CO_2$ reduces reaction rates, thereby resulting in poor combustion efficiency and reduced burning velocities [20–22]. Therefore, the mixing

of a higher flame speed fuel with base fuel is advantageous. Hydrogen has been historically used as rocket propellant due to its higher flame speed, and its addition with hydrocarbon fuel results in cleaner flames with wider flammability limits [23]. Hydrogen is being considered as a potential energy carrier because of its range of advantages, as it projects to play a vital role as a fuel additive with natural hydrocarbons in gas turbines and internal combustion engines.

Research community is foreseeing the use of hydrogen-blended fuels as one of the promising alternatives of the natural gas in combined cycle power generation cycles [24–26]. Several studies have shown that hydrogen-enrichment of the conventional fuels considerably reduces soot formation and $CO_2$ emissions [27,28]. Others have reported wider lean flammability limits and increased laminar flame speed for hydrogen-enriched flames [29–33]. Furthermore, both the average and the instantaneous characteristics of premixed turbulent flames are affected with even very minute addition of hydrogen concentration to the basic fuel [34]. Although widespread investigation has been performed on air-based combustion of hydrogen enriched methane (such as [35]), hydrogen-enrichment of oxy-fuel flame still requires further research to justify its role in a process that is preferably carried out at near stoichiometric conditions.

## 1.6 Problem Statement

There is scarce understanding of stable combustion zones pertaining to the premixed $CO_2$-diluted oxy-propane flames ($C_3H_8/O_2/CO_2$) and oxygen-enriched air-based propane flames ($C_3H_8/O_2/N_2$). The knowledge of stability and combustion characteristics of these flames will aid gas turbine designers and operators in prospective shift toward oxy-fuel and

enhanced-$O_2$ combustion. The present work endeavors to fill this gap by investigating the stability and flame macrostructures of propane-based flames.

In addition, the stability of premixed hydrogen-enriched $CO_2$-diluted oxy-methane ($CH_4/H_2/O_2/CO_2$) flames have been investigated but there is a shortage of understanding in terms of the influence of oxygen fraction (*OF*) on flame structure and pertaining emissions on these hydrogen-enriched flames. Therefore, this study also incorporates large eddy simulations (LES) for investigating the performance of $CH_4/H_2/O_2/CO_2$ flames.

## 1.7 Objectives

The objectives of present thesis work include,

1. Investigation of the stable range of combustion for $C_3H_8/O_2/N_2$ and $C_3H_8/O_2/CO_2$ flames for a range of *OF* and equivalence ratio ($\varphi$).
2. The characterization of a range of combustible mixture needs to be carried with studying the influence of various parameters.
3. The effects of hydrogen fraction (*HF*), *OF* and bulk throat velocity ($U_{in}$) on combustion and emission attributes of $CH_4/H_2/O_2/CO_2$ flames are aimed to be numerically investigated.

## 1.8 Organization of the work

This thesis work includes eight chapters. It starts from discussing the main topic of the study introduced in Chapter 1, which comprises of basic theories which lay foundation for the formation of basic building blocks. Chapter 2 comprehensively considers the available till-date understanding of targeted area of the present study through literature review.

Chapter 3 presents the experimental and numerical model setup, along with test conditions used for this investigation. Chapter 4 illustrates and analyzes the findings related to the stability and macrostructure of $C_3H_8/O_2/N_2$ and $C_3H_8/O_2/CO_2$ flames. It also encompasses results and discussion on combustion and emission characteristics of $CH_4/H_2/O_2/CO_2$ flames. Chapter 5 sums up the key findings of this investigation with concluding remarks. In the end, Chapter 6 describes the future framework of the present study.

# CHAPTER 2

# LITERATURE REVIEW

Previous studies on oxy-fuel combustion were majorly inclined towards coal combustion, as it is a carbon rich fuel and burning it alone with oxygen results in increased concentration of waste $CO_2$, which consequences in increased carbon capture efficiency [36,37]. Majority of these oxy-fuel studies dealt with non-premixed and partially premixed conditions, while influence of swirler has also been included. Tamallah et al. [38] contrasted lean premixed swirl stabilized air and oxygen-based methane flames. Adiabatic flame temperature (*AFT*) of oxy-methane and air-methane combustion was matched by adjusting the dilution ratio in oxy-fuel mixture. Strouhal number's (based upon the flow inlet velocity and the azimuthal spinning frequency of outer recirculation zone) value was reported to be constant, irrespective of the inlet *Re*, at about 0.12 for both the oxygen and air-based flames. It was therefore concluded that *Re* is not the governing parameter for maintaining similar flow conditions in outer recirculation zone; instead, inlet flow velocity of mixture controls it. This finding persuaded to conduct the current experiments at fixed inlet velocity. Tamallah et al. [38] observed that single relationship exists between characteristic flame time (the reciprocal of extinction strain rate) and characteristic flow time (reciprocal of spinning frequency) in both air and oxygen-based flames.

## 2.1 Effects of Oxygen-enrichment on combustion characteristics

Research on temperature distributions, heating rate, fuel consumption and emissions with changing $O_2$ concentration from 21-30% was carried out by Wu et al. [39]. They studied

$O_2$ enrichment effects by using the furnace-temperature fixing and heating tests. They reported that amount of the time required for reaching 1200$^oC$ was 46% lesser for 30% $O_2$, as compared to 21% $O_2$ enrichment, signifying the enhanced heat transfer rate with increasing $O_2$ concentrations. During the transition from 21-30% of $O_2$ concentration, $NO_x$ emissions rose up by about 4.4 times and $CO_2$ concentrations also showed linear increments. It was also reported that air/fuel mixture with $O_2$ concentration of 30% consumed 26% lesser fuel as compared to the air/fuel mixture with $O_2$ concentration of 21%. Merlo et al. [40] studied the role of $O_2$-enrichment on pollutant emissions and stability of diffusion methane-air swirl stabilized flames. The reported that increasing $O_2$ concentrations highly encourages CO conversion to $CO_2$ and more $NO_x$ emissions were formed because of higher temperatures in the combustor. Moreover, it was reported that even with the low $O_2$ enrichment proportions, the flame stability got increased. Daood et al. [41] used coal air-staged combustion for studying the effects of $O_2$ enrichment on carbon burnouts and NO reduction. They reported that $O_2$ enrichment improves the carbon burnouts. In addition to it, at 31% of staging the experiments revealed that there was approximately 7% NO reduction with 28% of $O_2$ enrichment, whereas 35% NO reduction with 35% of $O_2$ enrichment, revealing an increase in NO reduction with greater concentrations of $O_2$. Tan et al. [42] studied enriched $O_2$ and $O_2/CO_2$ combustion in a down-fired vertical combustor. They reported that higher temperatures of flame and elevated concentrations of $O_2$ resulted in very high levels of $NO_x$. However, $O_2/CO_2$ flames suppressed $NO_x$ formation because of the unavailability of $N_2$ and very minute level of $NO_x$ was traced due to the air leakage at the fan. Horbaniuc et al. [43] studied OEC effects in large steam boilers. They reported an increase of about 2-5% in the boiler efficiency,

because of high temperatures of flue gases. This higher mean logarithmic temperatures within the heat exchangers cause reduction of the heat transfer surfaces. Qiu and Hayden [44] explored membrane separation for air-enrichment and investigated the impact of OEC on natural gas flames in porous ceramic radiant burners. Polymer membranes were utilized for passive production of $O_2$-enriched air, and $O_2$ was enriched from 21% to 28%. Their experimental results revealed that $O_2$ enrichment of air of 28% reduces about 22% of the natural gas consumption. Lambert et al. [45] studied OEC impacts on steam methane reforming using membrane separation technique for air-enrichment. They reported that an optimum $O_2$ enrichment of air is 29% for steam methane reforming.

## 2.2 Flame Speed dependence on Adiabatic Flame Temperature

While air-based fossil fuel combustion has already been utilized in the industry and focus is now being shifted towards oxy-fuel combustion and $O_2$ enriched air-fuel for cleaner and efficient energy conversion. As review has defined examples of different fuels burnt with excessive $O_2$ concentration air using different combustion techniques, all these studies have followed similar characteristic that increasing $\varphi$ of reacting mixture increases both flame speed *LFS* and *AFT*. According to Kaskan [46], the maximum *LFS* of propane-air flame was reached at $\varphi$ = 1.1 and drops for all other richer and leaner mixtures. Kaskan [46] and Van Maaren et al. [47] after conducting investigations on various fuels presented a relationship between *AFT* and *LFS* as log (*LFS*) $\alpha$ 1/*AFT*. Moreover, this relation was found to be valid for both liquid [48] and gaseous [49] fuels. It was reported that preheating the reactants mixture increases *LFS*. The dilution of mixture with $H_2O$, argon, $CO_2$, helium, or $N_2$ decreases the *AFT* and therefore *LFS* is reduced. Due to the importance of *AFT* in

controlling flame dynamics, the present study investigates the influence of *AFT* on $CO_2$ and $N_2$ based premixed propane flames.

Shroll et al. [50] studied the dynamic stability features of oxy-methane flames. They used *OF* for controlling *AFT*. Although the burning velocities of both air and oxygen-based flames are quite different for a specific *AFT* value, but still both of these flames were similar in the fact that *AFT* of the reactant mixture controls the movement from one stability point to the other. Since turbulent flame geometry is a strong function of *AFT*, they reinforced this finding by showing high-speed images of the comparable vortex breakdown modes, which was representing similar turbulent flame geometries. Kutne et al. [51] used swirl stabilized model combustor used for gas turbines for comparing the partially premixed oxygen and air-based methane flames. They considered range of 0.5-1 for $\varphi$ and 20%-40% for *OF*. It was concluded that the flame characteristics are strong function of the *OF*, while $\varphi$ affects them only slightly. This finding influenced the investigation of the *OF* effects on $CH_4/H_2/O_2/CO_2$ flames. Moreover, they reported that inner recirculation zone of the oxy-flames was existing further downstream in contrast to the air-based ones, representing the inferior stability of oxy-flames. This comparison of the flame characteristics for air and oxy-propane flames have been rarely investigated, as per the literature review and motivated experimental investigation of the flame stability and macrostructure of $C_3H_8/O_2/CO_2$ and $C_3H_8/O_2/N_2$ flames in this thesis work.

## 2.3 Propane-based Combustion

Propane $C_3H_8$ has been used as vehicle fuel, propellant, refrigerant and petrochemical feedstock. It is a key component of Liquefied Petroleum Gas (LPG) and its utility for heating and cooking purposes is significant. Although its concentration in natural gas is

minor yet it is sensitive to overall combustion performance. With growing energy demands, depleting fossil fuel reserves and endeavors for cleaner environment, the knowledge of combustion performance of $CO_2$ and $N_2$ based propane mixture cannot be neglected. Chu et al. [52] investigated $O_2$ enrichment effects on soot formation with diffusion propane flames. Their analysis conveyed that $O_2$ enrichment increases combustion temperature and also broadens up the soot formation region, resulting in increased volume fraction of soot particles. Abubakar et al. [53] studied $C_3H_8/O_2/CO_2$ diffusion flames and reported that as $CO_2$ dilution increases 40%, the flame shape changes from jet like shape to lifted V-structured shape. The characteristics of premixed propane flame have been rarely investigated and the current study therefore focuses at investigating the stability of premixed $C_3H_8/O_2/CO_2$ and $C_3H_8/O_2/N_2$ flames.

Due to varied combustion behavior of different fuels along with their subsequent different emissions characteristics, the stability performance of flames changes with variations in reactant loading conditions. Therefore, the design and development of fuel-flexible burners is necessitated so that, different flames with different loading conditions under lean premixed oxy-fuel and $O_2$-enriched air-fuel combustion conditions can have sustainable and stable flames. The combustion behavior of propane-based flames needs further investigation, especially in terms of flame stability and combustion characteristics, as it has been rarely studied so far. This study aims to fill this gap and investigate the combustion performance of these flames in a dry low emission (DLE) lean premixed (LPM) swirl stabilized model combustor for giving an insight to designers and operators of its stable flame behavior. The advantages of $O_2$-enriched air-propane and oxy-propane combustion can be harnessed by having fuel-flexible gas turbines with minimal retrofitting. In this

study, the stability and structure of these flames are investigated at fixed mixture inlet velocity of 5.2 m/s for DLE model combustor of gas turbines, ranging the equivalence ratio from 0.1 to 1.0 and oxygen fraction from 21% to 70%.

## 2.4 Effects of Hydrogen-Enrichment on Oxy-Methane Flames

Researchers are aiming for carbon-free fuels for mitigating the hazardous effects of greenhouse gases on our environment. Hydrogen has been used as a rocket-propellant and has the potential of efficient and environmentally friendly energy conversion. One portion of the present work comprises on the effects of *HF*, *OF* and $U_{in}$ on the combustion phenomena of $CH_4/H_2/O_2/CO_2$ flames using LES.

Hu et al. [54] and Sarli et al. [55] examined the influence of hydrogen-enrichment on laminar flame speed (*LFS*) and reported a linear correlation between them. Tang et al. [56] also reported that hydrogen-enrichment of fuel blend enhances both unstretched laminar flame propagation and flame speed. Moreover, they noticed that dependence of these properties is more notable at higher hydrogen fractions (*HFs*) in the fuel blend. Sankaran and Im [57] and Hu et al. [54] reported that augmented molecular diffusivity of $H_2$ and enhanced formation of radicals (such as H, O and OH) are main reasons behind improved *LFS* of hydrogen-enriched flames. Nakahara et al. [58] observed a monotonic increase in turbulent flame speed (*TFS*) with hydrogen-enrichment in a lean combustible mixture. An analogous behavior has been described by Halter et al. [34] for *TFS* of hydrogen-enriched premixed methane/air flames. They also showed that hydrogen-enrichment enhances the turbulent flame speed ($S_T$) more readily than the corresponding *LFS*, thereby resulting in an overall higher combustion intensity ($TFS/FS$). Danielle et al. [59,60] also confirmed

these findings and stated that hydrogen-enrichment slightly increases the flame front curvature distribution, thus augmenting the small scale flame wrinkling which consequently yields higher *TFS*. The chemical behavior of $CO_2$ in lean to stoichiometric $CH_4/H_2/O_2/CO_2$ mixtures were investigated by Liu et al. [61]. They identified significant reduction in *LFS* with elevating concentrations of $CO_2$ in oxidizer mixture. They also reported reaction between atomic hydrogen and $CO_2$ as a mitigation factor for dominant radicals (i.e. H, O and OH), which subsequently retards the *LFS*. Schefer [62] experimentally studied the stable behavior of hydrogen-enriched flames. He reported that the lean blowout (*LBO*) limit was maximum with stoichiometric conditions and it was reduced for both rich and lean mixtures. In addition, *LBO* limit was reduced by nearly 15% and OH mole fraction was increased by almost 20% with hydrogen addition of about 20% (by vol.) in the fuel mixture. Although hydrogen addition decreases *AFT* of the flame but due to its higher combustibility, higher reaction zone temperatures are reported for the flames with higher *HFs*. Fast expansion of reaction zone results due to elevated temperature and therefore inhibits cooler recirculation flow [23].

Cheng and Littlejohn [63] studied the combustion features of pure hydrogen-dilution of air and $H_2$-$N_2$ mixture in a laboratory scale low swirl injector (LSI) for implementation in integrated gasification combined cycle (IGCC) gas turbines. With variable bulk velocities in the system, the study found that LBO limit is reached nearly at a fixed equivalence ratio ($\varphi$) of 0.17 indicating the independency of LBO limit with varying Reynolds number (*Re*). Damköhler number (*Da*) was found to be another parameter which successfully predicts the LBO limit. In addition, an interesting finding explained that different combinations of $CH_4/CO/H_2$ concentrations reach LBO at a constant Damköhler number of 0.4. Similar

conclusion was reported in one of our previous studies on the current combustor model of gas turbine [64]. It was found that *LBO* limit occurs at fixed *AFT*. This indicates that *AFT* is a more appropriate factor choice than $\varphi$ or oxygen fraction (*OF*) for quantification of static stability map of the combustor.

Suliman et al. [29] investigated role of hydrogen-enrichment and inlet velocity of the reactants premixed $CO_2$ diluted oxy-methane flames. It was reported that the hydrogen addition results in reducing the size of flames; representing improvement in reaction chemical kinetics. Stable range of combustion for these flames were identified by quantifying flashback and blowout extinction limits.

Nemitallah et al. [65] carried out numerical and experimental investigation for studying influence of hydrogen-enrichment and inlet velocity of the premixed hydrogen enriched $CO_2$ diluted oxy-methane flames. They reported that chemical kinetics reaction rate dominates the reaction and turbulence does not alter the macrostructure of the flame. They further reported that hydrogen addition results in wider operability range and improved heat release rates.

The thesis work aims at experimental and numerical investigation of flame behavior and attributes, as well as the emission features of the premixed $CO_2$-diluted hydrogen-enriched oxy-fuel flames in a premixed dry low emission (*DLE*) swirl combustor – a topic of emerging interest that has been rarely investigated. The investigation was performed under stoichiometric combustion conditions to make perfect use of oxygen in order to translate oxy-combustion in an inexpensively feasible process. The study explores the flame behavior for a range of *HF*, *OF* and bulk throat velocity ($U_{in}$) of the mixture. The role of

the *OF* has not yet been studied for hydrogen-enriched flames, as per the review and knowledge of authors. The present investigation sheds light on influence of the *OF* on premixed $CH_4/H_2/O_2/CO_2$ flames, which also was not addressed in the investigations of Suliman et al [29] and Nemitallah et al [65]. Furthermore, emissions characteristics owing to changes in *HF*, *OF* and $U_{in}$ are reported in the current study, which makes this investigation novel. The current measurements and subsequent analysis provide useful information for minimizing the adaptability and retrofitting issues of existing air-fuel gas turbines to reduced emission hydrogen-enriched oxy-fuel turbines.

# CHAPTER 3

# EXPERIMENTAL AND NUMERICAL MODEL

## 3.1 Experimental Setup for $C_3H_8/O_2/CO_2$ and $C_3H_8/O_2/N_2$ flames

### 3.1.1 Combustor Model Specifications

The LPM DLE swirl stabilized premixed fuel-flexible model gas turbine combustor was used for examining premixed $C_3H_8/O_2/CO_2$ and $C_3H_8/O_2/N_2$ flames for clean and efficient power production. The schematic diagram of combustor setup, with the combustor headend at the top is shown in Figure 2.1. The power density range of operational gas turbines is usually 3.5-20 MW/$m^3$/bar and therefore, this experimental gas turbine combustor follows the same. Static stability of the $O_2$ enriched flames was found with the help of two flame extinction limits i.e. blowout and flashback limits. Experiments were performed with non-preheated atmospheric pressure containing reactants with fixed inlet bulk velocity.

A 55$^o$ geometric swirler was installed on the combustor for providing swirl effect to the premixed reactants of controlled composition. After swirler, flow of reactants was accelerated as it passed through a converging-diverging throat insert with diameter of 2.0 cm placed in the immediate downstream of swirler. For reduction in swirl loss, insert gave gradual convergence of 30$^o$ to the flow and then for the prevention of its sudden expansion downstream, 45$^o$ divergence was induced. A quartz tube was placed at the top of combustor headend for confining $O_2$ enriched flames from atmospheric air.

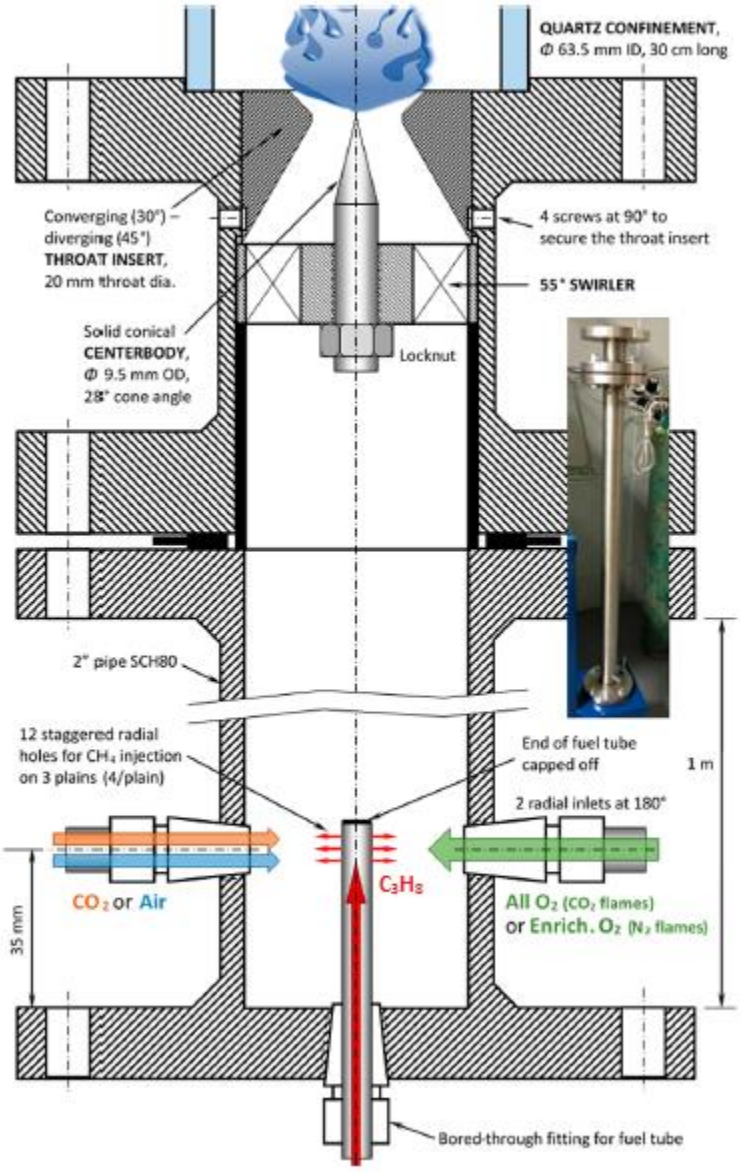


**Figure 2.1 - Model gas turbine combustor schematic used for experiments.**

The flow velocity at the throat was balanced by the flame velocity for achieving stable flame behavior, as it has been defined previously as an important characteristic for achieving stable flames [66]. Flashback can also be resulted because of vortex breakdown so a conical solid bluff body was fitted in the centerline of the burner.

Below the swirler inlet, a premixed reactant mixture was composed by injecting air, $C_3H_8$ and $O_2$ gases in mixing pipe of 1.0 m length and 2.0-inch diameter. Aalborg Inc. thermal

mass flow controllers of ±0.5% full-scale accuracy, were used for controlling the gas flow rates, with an uncertainty of ±0.4% in *OF* and ±0.02 in $\varphi$. The mixing plenum of an aspect ratio (length/diameter) of about 20 was used for ensuring maximum premixing of the reactants in the pipe. The oxidizer gases i.e. air and $O_2$ were injected from opposite sides, while fuel gas i.e. $C_3H_8$ was added by a tube placed in the center of pipe. This tube was packed from its top and 12 radial holes arranged in three consecutive planes were used for diffusing fuel in the mixing pipe. These holes of fuel inlet were aligned with oxidizer inlets of air and $O_2$ gases. Although, direct measurement of degree of premixing of the reactants was not carried out but a test was conducted for evaluating the effectiveness of premixing. This test comprised on different stable flames of varied compositions. From the reference position shown in Figure 2.1, the axial location of fuel inlet holes present in the tube was varied from +100 mm to -25 mm. Corresponding aspect ratio was changed from 18.5 to 20.5. The change in holes location shown no discernible effects on flame color, noise, shape and size, which implied perfect premixing of the reactant mixture. All of the investigated flames possessed a constant inlet velocity of 5.2 m/s for entire examined compositions of the premixed reactants. For safety reasons, an emergency shut-off valve was installed in fuel line for promptly cutting down fuel supply on reaching flashback limit.

The changes in the visual flame appearance indicated the changes in the operating parameters during experiments. Flame shape analysis was carried out with photographic flame images taken by a 24 MP camera of 1600 ISO, 5.6 f-stop and 1/60-s shutter speed features.

A thermocouple of 1.0 mm junction diameter and of R-type (PtRh13%-Pt) from Omega was incorporated for measuring local mean temperature inside quartz confinement. At each

location, the average temperature is measured with multiple readings with the help of thermocouple probe, which is connected to a data logger and a computer. A traverse mechanism is incorporated for precise axial and radial movements of thermocouple probe, which enters in the confinement from top of the tube.

The model by Brohez et al. [67] was, then, used for correction of the radiation errors to the surroundings. Measurements of axial (through centerline of the combustor) and radial (at heights of 10.0 cm and 20.0 cm from the combustor throat) temperature distributions for selected flames were performed. For further details of experimental procedure and setup , reader is referred to one of the previous studies of the Authors [68].

### 3.1.2 Test Conditions and Governing Equations

The premixed $C_3H_8/O_2/CO_2$ and $C_3H_8/O_2/N_2$ flames are investigated at constant inlet velocity in present study. Considerable differences in the macrostructure and operability limits of the flames are expected due to the involvement of different diluents ($CO_2$ and $N_2$). The terms of "bulk throat velocity" and "bulk *Re*" refer the quantities of all participating reactants in $C_3H_8/O_2/CO_2$ and $C_3H_8/O_2/N_2$ flames and not $C_3H_8+O_2$ alone.

The Authors [69] have examined $CH_4/O_2/CO_2$ flames previously and a thorough description of approach for keeping the inlet velocity fixed at 5.2 m/s has been provided. The following species flow rates are found by using this generalized approach for a diluent X, which is either $N_2$ or $CO_2$.

$$\dot{m}_{C_3H_8} = 44\left(\frac{pAv_a}{R_uT}\right)\left(1+\frac{2}{OF\varphi}\right)^{-1} \tag{3.1.1}$$

$$\dot{m}_{O_2} = 64\left(\frac{pAv_a}{R_uT}\right)\left(\varphi + \frac{2}{OF}\right)^{-1} \quad (3.1.2)$$

$$\dot{m}_X = 2M_X\left(\frac{pAv_a}{R_uT}\right)\left(\frac{1-OF}{\varphi OF+2}\right) \quad (3.1.3)$$

Therefore,

$$\dot{m}_{N_2} = 56\left(\frac{pAv_a}{R_uT}\right)\left(\frac{1-OF}{\varphi OF+2}\right) \quad (3.1.3a)$$

And

$$\dot{m}_{CO_2} = 88\left(\frac{pAv_a}{R_uT}\right)\left(\frac{1-OF}{\varphi OF+2}\right) \quad (3.1.3b)$$

Where $\varphi$ and *OF* are examined over the ranges of 0.1-1.0 and 21%-70% respectively.

It is important to mention about eq. 3.1.1 that the diluent (X) properties do not affect the propane gas mass flow rate $\dot{m}_{C_3H_8}$; i.e. the similar amount of fuel is consumed for both test sets of common *OF* and $\varphi$. In addition, oxygen-enrichment of pure air flow is performed for producing desired $O_2/N_2$ diluted oxidizer mixture with any *OF*. The required air flow rate is calculated as follows, by using $\dot{m}_{N_2}$ from eq. 3.1.3a and the fact that by mass, air consists of 76.7% nitrogen

$$\dot{m}_{Air} = \frac{\dot{m}_{N_2}}{0.767} \quad (3.1.4)$$

Depending on eq. 3.1.2, 3.1.3a, and 3.1.4, enriched oxygen flow rate is determined as

$$\dot{m}_{enO_2} = \dot{m}_{N_2} + \dot{m}_{O_2} - \dot{m}_{Air} \quad (3.1.5)$$

The dynamic viscosity of bulk reactant mixture is calculated as follows [70]

$$\mu_{mix} = \frac{\sum y_i \mu_i \sqrt{M_i}}{\sum y_i \sqrt{M_i}} \quad (3.1.6)$$

Likewise, its bulk density is calculated by using the following formula

$$\rho_{mix} = \frac{P \sum \dot{m}_i}{R_u T \sum (\dot{m}_i / M_i)} \quad (3.1.7)$$

The Reynolds number at the throat of the burner is calculated as

$$Re = vD\rho_{mix}/\mu_{mix} \quad (3.1.8)$$

The exhaust gas composition and *AFT* are dependent on both *OF* and $\varphi$ of the reactant mixture. Moreover, with the help of tabulated enthalpies of formation for $C_3H_8$, $N_2$ and $O_2$ and sensible (temperature dependent) enthalpies of $CO_2$, $O_2$, and $H_2O$ [71], the thermodynamic analysis is carried out for calculating *AFT*.

### 3.1.3 Experimental Procedure

With fixed bulk inlet velocity, mass flow rates of individual reactants were changed and mutually adjusted according to a specific data point (with definite *OF* and $\varphi$). *OF* ranged from 21% to 70% while $\varphi$ was fluctuated from 0.1 to 1.0. For every *OF* representing a unique flame, following procedure was followed for investigating blowout and flashback extinction boundaries.

(a) As a first step, flame was ignited at a safe ignition point, away from both flashback and blowout extinction limits.

(b) For reaching the required data point indicated by distinct *OF* and $\varphi$, mass flow rates of individual reactants were adjusted. For a fixed *OF*, richer $\varphi$ was sought if flashback extinction limit was required and similarly leaner $\varphi$ was hunted for the flame to extinct

with blowout. Higher audible noise and jet like flame shape attached to the throat of the combustor were observed to be the indication that flame is near its flashback limit. Weaker lifted flames represented the vicinity of blowout extinction limit.

(c) At a specified *OF*, $\varphi$ was made cautiously leaner and flame started to become weak and lifting up from the throat surface, until it reached till blowout limit and this specific combination of the *OF* and $\varphi$ was noted as a blowout extinction point.

(d) After it, stable flame was ignited and richer $\varphi$ was sought. As flame started to emit audible noise, gradual movement was made with smaller careful transitions especially near the flashback limit. At the point of flashback limit, audible noise reached its maximum level accompanied by an explosion and flame flashed back to the burner throat. This specific $\varphi$ was noted with *OF* as a flashback extinction point.

(e) Steps from (a) to (e) were repeated again for the complete range of the *OF*. Static stability map was plotted for both blowout and flashback limits, by connecting the highlighted blowout $\varphi$ point of different *OF* domain and similarly by joining the nominated flashback $\varphi$ points.

## 3.2 Numerical Model Setup of $CH_4/H_2/O_2/CO_2$ flames

The numerical simulations were performed with $CH_4/H_2$ fuel and $O_2/CO_2$ oxidizer mixtures at atmospheric pressure and stoichiometric condition. The power density of model combustor mimics the operation range from 3.5 to 20 $MW/m^3/bar$, which is typical of operational gas turbines. Numerical simulations of the test cases are performed for a range of *HF* ( from 20% to 60% by vol.), *OF* (from 30% to 38% (by vol.) and $U_{in}$ (from 4.4 m/s to 6.0 m/s).

### 3.2.1 Equations of Conservation

The incorporated mathematical model solves the species transport equation and conservation equations of mass, momentum and energy using large eddy simulation (*LES*) model for scalar variables within three-dimensional (*3D*) region representing the model gas turbine combustor. Commercial software package of ANSYS-Fluent 19.2 was utilized for carrying out simulations. Heat transfer, emission characteristics, and flow regime of $CH_4/H_2/O_2/CO_2$ flames were forecasted by simultaneously solving the elliptic equations in 3D domain. Species transport equation and conservation of mass, momentum, and energy equations are based on the following general equation [72]:

$$\frac{\partial}{\partial x_J}\left(\bar{\rho}\,\overline{U_J}\emptyset + \bar{\rho}\,\overline{u_J}\bar{\varphi}\right) = \frac{\partial}{\partial x_J}\left[\Gamma_\varphi \frac{\partial \emptyset}{\partial x_J}\right] + \rho\overline{S_\emptyset} \tag{3.2.1}$$

where $\emptyset$ and $\varphi$ represent Reynolds average and fluctuating components of dependent variable, respectively, $u_J$ is the velocity component in *J* direction, $\Gamma_\varphi$ is diffusion component, whereas $S_\emptyset$ represents source term.

### 3.2.2 Radiation Model

Discrete ordinate (*DO*) model was incorporated for solving radiation heat transfer equation such that with every five energy iterations there is one radiative iteration. *DO* model thicknesses has been recommended for modeling oxy-fuel combustion [73] and it is valid for wide range of optical. The absorption coefficient, which is verified over a broad range of operating conditions of gaseous mixture, was calculated with the weighted sum of grey gas model (*WSGGM*) [74,75].

### 3.2.3 Turbulence Model

Large eddies represent the characteristic length of mean flow, whereas small eddies dissipate the turbulence kinetic energy, and jointly they approximate turbulence in the flow. In this study, turbulence was solved by the LES modeling technique, where small eddies were filtered out. Low-pass filtering operation was considered by utilizing the following equation for a quantity [65]:

$$\bar{\varphi}(x,t) = \int G(r,x)\varphi(x-r,t)dr \tag{3.2.2}$$

This equation solves integration for the entire domain. The scale of the resolved eddies is determined by filter function, $G$. Following forms of general equations are yielded using continuity, Navier-Stokes equations, and filtering function:

$$\frac{\partial \rho}{\partial t} + \frac{\partial}{\partial x_i}(\rho \bar{u}_i) = 0 \tag{3.2.3}$$

$$\frac{\partial}{\partial t}(\rho \bar{u}_i) + \frac{\partial}{\partial x_j}\left(\rho \bar{u}_i \bar{u}_j\right) = \frac{\partial}{\partial x_j}\left(\mu \frac{\partial \sigma_{ij}}{\partial x_j}\right) - \frac{\partial \bar{p}}{\partial x_i} - \frac{\partial \tau_{ij}}{\partial x_j} \tag{3.2.4}$$

where $\sigma_{ij}$ represents the stress tensor (because of the molecular viscosity), defined by:

$$\sigma_{ij} \equiv \left[\mu\left(\frac{\partial \bar{u}_i}{\partial x_j} + \frac{\partial \bar{u}_j}{\partial x_i}\right)\right] - \frac{2}{3}\mu \frac{\partial \bar{u}_i}{\partial x_j}\delta_{ij} \tag{3.2.5}$$

The subgrid-scale stress $\tau_{ij}$ is given by:

$$\tau_{ij} \equiv \rho\overline{u_i u_j} - \rho \bar{u}_i \bar{u}_j \tag{3.2.6}$$

Filtering operation results in subgrid-scale stresses, which involve modeling. Isotropic part of the subgrid-scale stress and filtered static pressure terms are therefore merged and modeling of deviator part is carried out by using turbulent viscosity:

$$\tau_{ij} = -2\mu_t \bar{S}_{ij} \tag{3.2.7}$$

where $\mu_t$ and $\bar{S}_{ij}$ are the turbulent viscosity and rate of stain tensor, respectively. Wall-Adapting Local Eddy-viscosity (WALE) model was used for solving the turbulent viscosity, and is given by:

$$\mu_t = \rho L_s^2 \frac{\left(S_{ij}^d S_{ji}^d\right)^{3/2}}{\left(\bar{S}_{ij}\bar{S}_{ji}\right)^{5/2} + \left(S_{ij}^d S_{ji}^d\right)^{5/4}} \tag{3.2.8}$$

where $L_s$ symbolizes mixing length for subgrid-scale.

Both $L_s$ and $S_{ij}^d$ are given as:

$$L_s = \min\left(\kappa d, C_w V^{1/3}\right) \tag{3.2.9}$$

$$S_{ij}^d = \frac{1}{2}\left(\bar{g}^2{}_{ij}\bar{g}^2{}_{ji}\right) - \frac{1}{3}\delta_{ij}\bar{g}_{kk}^2 \tag{3.2.10}$$

where $\kappa$ is denotes von Karman constant. WALE constant is given by $C_w$, d represents distance to closest wall, and $V$ is volume of computational cell. $\bar{g}_{ij}$ is defined as:

$$\bar{g}_{ij} = \frac{\partial \bar{u}_i}{\partial x_j} \tag{3.2.11}$$

### 3.2.4 Reaction Kinetics Model

Fully premixed combustion case for hydrogen-enriched oxy-methane simulations was accommodated with modified partially premixed combustion model. The transport equations for the mean mixture fraction $\bar{f}$, the mixture fraction variance $\overline{f'^2}$ and the mean reaction progress variable $\bar{c}$ were computed for obtaining additional scalar variables. The reaction progress variable is defined as the mass fraction of specific species in the mixture and possesses a value of 1.0 for burnt gas mixture and zero for unburnt mixture. Mixture fraction is given as:

$$f = \frac{sY_{fu} - Y_{ox} + Y_{ox,0}}{sY_{fu,1} + Y_{ox,0}} \tag{3.2.12}$$

where $Y$ represents the mass fraction with $Y_{fu}$ and $Y_{ox}$ symbolize the mass fractions of fuel and oxidizer. Subscripts 0 and 1 refer to the inlet streams of oxidizer and fuel, respectively, while $s$ represents oxidizer to fuel ratio. The probability density function and progress variable are computed with the distinct mixture fraction and the density weighted average scalars such as species fraction and temperature are computed based on following equation:

$$\overline{\emptyset} = \bar{c} \int_0^1 \emptyset_b(f) p(f) df + (1 - \bar{c}) \int_0^1 \emptyset_u(f) p(f) df \tag{3.2.13}$$

where u and b denote unburnt and burnt mixtures, respectively.

Reaction progress variable, $c$, is described as a function of mass fraction of product species and is given by:

$$c = \left( \frac{\sum_{i=1}^{n} Y_i}{\sum_{i=1}^{n} Y_{i,ad}} \right) \tag{3.2.14}$$

where subscripts $i$ and $ad$ represent the product and the complete combustion species, respectively.

Following correlation was used for estimating the flame thickness:

$$\delta = \frac{\lambda_u}{\rho_u c_p S_L} \tag{3.2.15}$$

where $\rho_u$ and $\lambda_u$ represent thermal density and conductivity, respectively.

The ratio indicating the rate of reaction to the rate of diffusion is given by Damköhler number:

$$Da = \frac{\left({}^{l_t}/_{u\prime}\right)}{\left({}^{\delta}/_{S_L}\right)} \tag{3.2.16}$$

where $l_t$ indicates the integral length scale and $u'$ represents the root mean square (*RMS*) of velocity fluctuation.

### 3.2.5 Boundary Conditions

For reducing the computational time, only an axis-symmetric quadrant of symmetric modeled reactor was considered for all the simulations as shown in Figure 2.2. After performing a mesh independency study, 40,000 finite volume cells were selected. This model was also used in one of the investigations carried by the authors [65]. Fine meshes were created near burner region whereas cruder meshes were generated in outlet and near outlet zone. Various compositions of $CH_4/H_2/O_2/CO_2$ with constant yet distinct throat velocity ($U_{in}$) were introduced in the combustor through the inlet. Tangential and axial components of flow were used for introducing a swirl flow of 0.98 swirl number [65].

Fluctuating velocity was solved by incorporating vortex method algorithm. According to set values of equivalence ratio and mixture composition, calculations were performed for the mean mixture fraction using the modified partially premixed model.

At the combustor wall, mixed thermal boundary condition was defined with both external radiation and convection heat transfer mechanisms, as well as convective heat transfer coefficient of 20 $W/m^2/K$ and free stream temperature of 300 K. The semi-transparent boundary type was set to the 6.0 mm wall thickness. The radiation heat transfer through the quartz confinement was estimated using non-gray band model with 4.0 wavelength bands. The tangential components of swirling flow were taken care with periodic boundary conditions, which were assigned to both symmetric faces of the considered quadrant portion of the combustor. All simulations were carried out at fixed equivalence ratio of 1.0 (stoichiometric condition) with varying *OF*, *HF* and $U_{in}$.

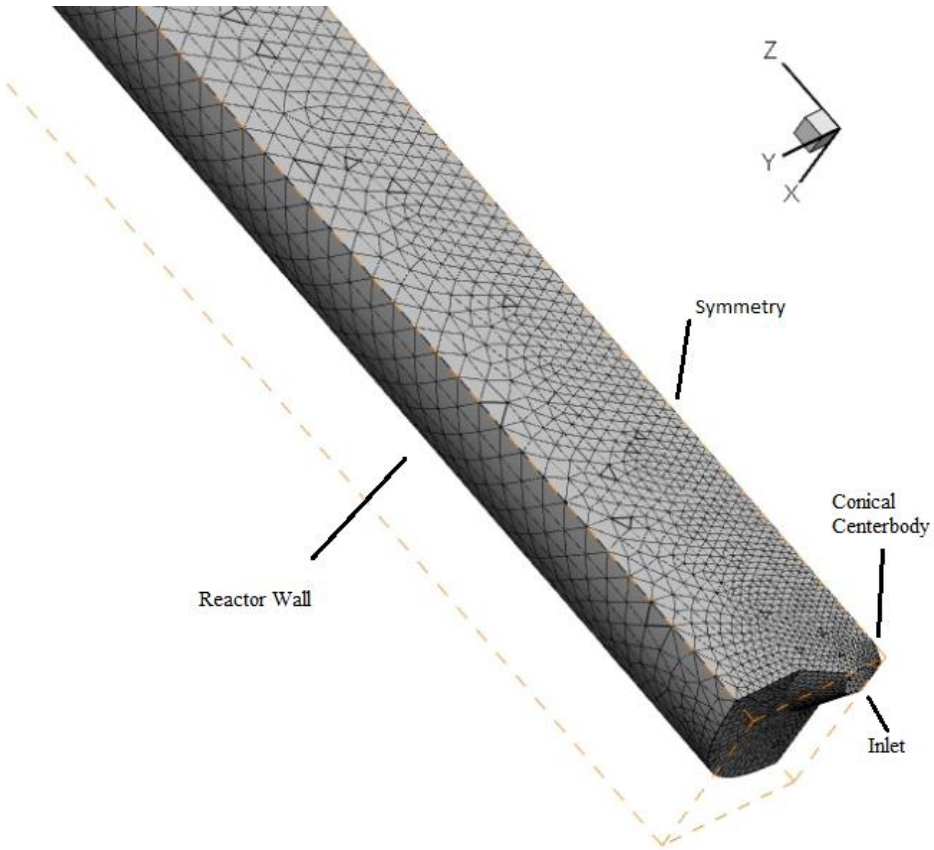


**Figure 2.2 - Combustor quadrant mesh used in the numerical calculations.**

# CHAPTER 4

# RESULTS AND DISCUSSION

## 3.1 Experimental Results of $C_3H_8/O_2/N_2$ and $C_3H_8/O_2/CO_2$ flames

### 3.1.1 Combustor Stability Maps

Oxygen and Nitrogen possess comparable properties i.e. nearly similar heat capacities and densities. It is thus expected that changes in the oxygen fraction (*OF*) of the diluted $O_2/N_2$ oxidizer mixture would not considerably affect the oxidizer properties. In contrast, $CO_2$ contains substantially different properties. It is therefore anticipated that *OF* would play an important role in oxy-fuel flames especially in affecting the important combustion parameters like adiabatic flame temperature (*AFT*), as it is vital for the premixed flames analyses and it will be discussed in this results section.

The stability of the premixed oxygen-enriched air-propane ($C_3H_8/O_2/N_2$) and carbon dioxide diluted oxy-propane ($C_3H_8/O_2/CO_2$) flames is quantified for DLE combustor of gas turbine over ranges of equivalence ratio (0.1-1) and oxygen fraction (21%-70%), at fixed inlet velocity of 5.2 m/s. Stability maps (blowout and flashback limits) are presented against the constant *AFT* curves. Figure 3.1 illustrates the obtained stability maps for the $N_2$ (top) and $CO_2$ (bottom) flames. The error bars have been added to each data point for experimental uncertainty analysis.

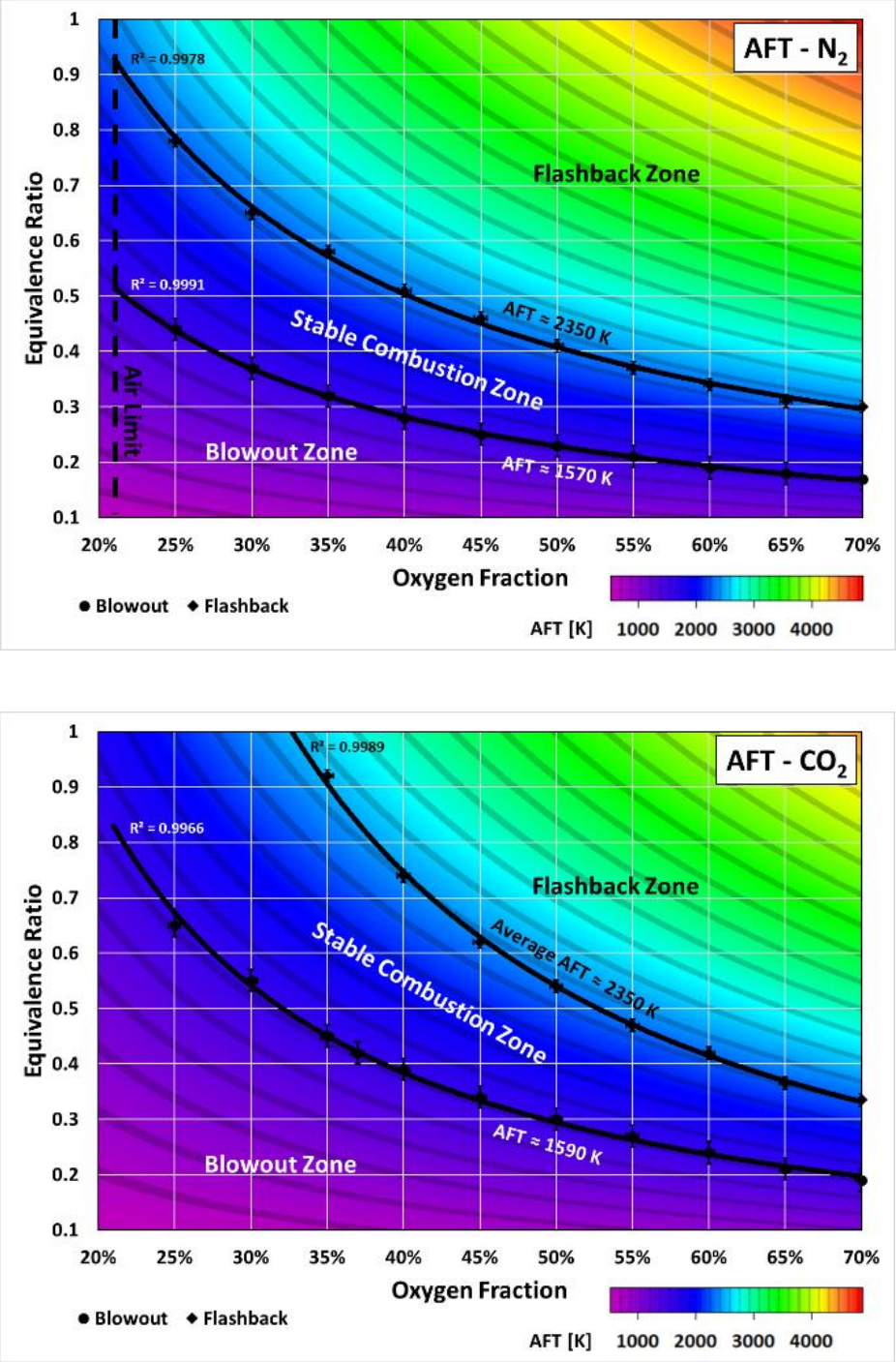


**Figure 3.1 - Combustor stability maps of $C_3H_8/O_2/N_2$ flames (top) and $C_3H_8/O_2/CO_2$ flames (bottom) along with constant *AFT* curves, with a throughout fixed inlet velocity of 5.2 m/s.**

For each *OF*, blowout point is designated by circular symbol, whereas flashback point is portrayed with diamond symbol. The exponential fits were observed for adequately representing blowout and flashback limits with $R^2$ values of 0.9991 and 0.9978, respectively for $N_2$ flames and 0.9966 and 0.9989, respectively for $CO_2$ flames. The area in between the fit lines represents the stable zone of combustion, while the areas below and above are the blowout and flashback zones respectively. For a one-to-one comparison, the colored backgrounds of constant *AFT* contours are presented at the same scale.

A primary observation of this study indicates that the blowout and flashback limits for both $CO_2$ and $N_2$ based flames follow the same *AFT* (Figure 3.1), for this specific case of constant inlet velocity of the premixed reactants. The slight deviation from *AFT* contour observed in $CO_2$ blowout and flashback limits is attributed to the error associating the simplified estimation of *AFT*; $CO_2$ flames have significantly more effluent $CO_2$ than $N_2$ flames; see Figure 3.2. If $CO_2$ dissociation was accounted for in *AFT*, the blowout and flashback limits would have followed a constant-*AFT* contour. Note that the mole fraction of effluent $CO_2$ increases along the flashback and blowout limits in direction of lower *OF*, and this region is exactly where the *AFT* error maximizes.

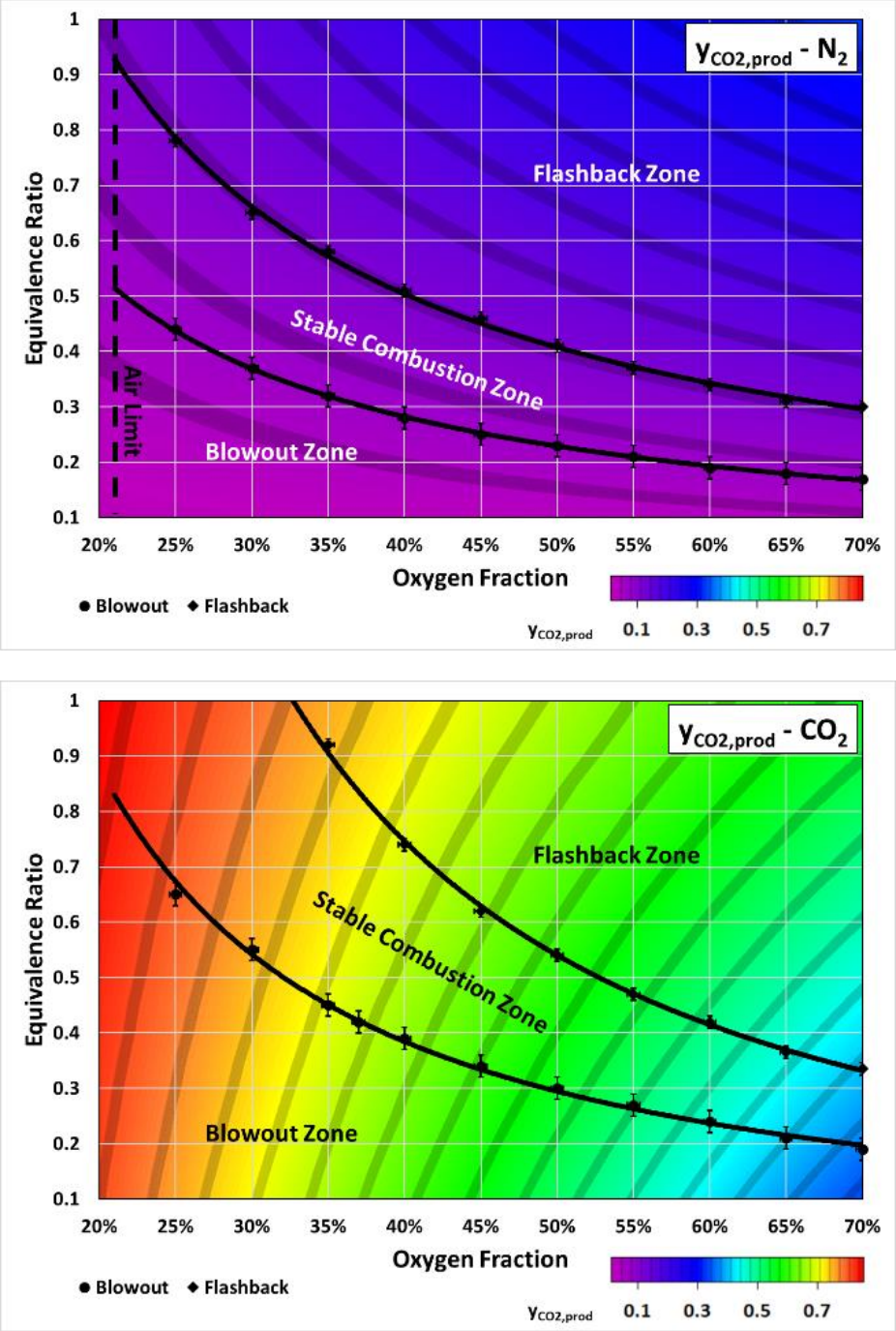


**Figure 3.2 - Static stability of the combustor plotted against the curves of $N_2$ mole fraction (top) and $CO_2$ mole fraction (bottom).**

The stability maps of the $CO_2$ and $N_2$ flames are plotted in Figure 3.3 for comparison. It indicates two preliminary observations. First, $CO_2$ flames possess steeper slopes of constant *AFT* contours $[\left(\frac{\partial \varphi}{\partial OF}\right) AFT]$. It indicates that *AFT* of oxy-propane flames is highly influenced by *OF*, as mentioned above. Second, the *AFT* of $CO_2$ flames is lower than that of $N_2$, for any specific set of *OF* and $\varphi$. The smaller heat capacity of $N_2$ in comparison to $CO_2$ is the reason for both observations. The static stability limits correlate well with *AFT* for both $CO_2$ and $N_2$ flames and it is a unique outcome for $C_3H_8$ flames and agrees with the previous findings for $CH_4$ flames [76].

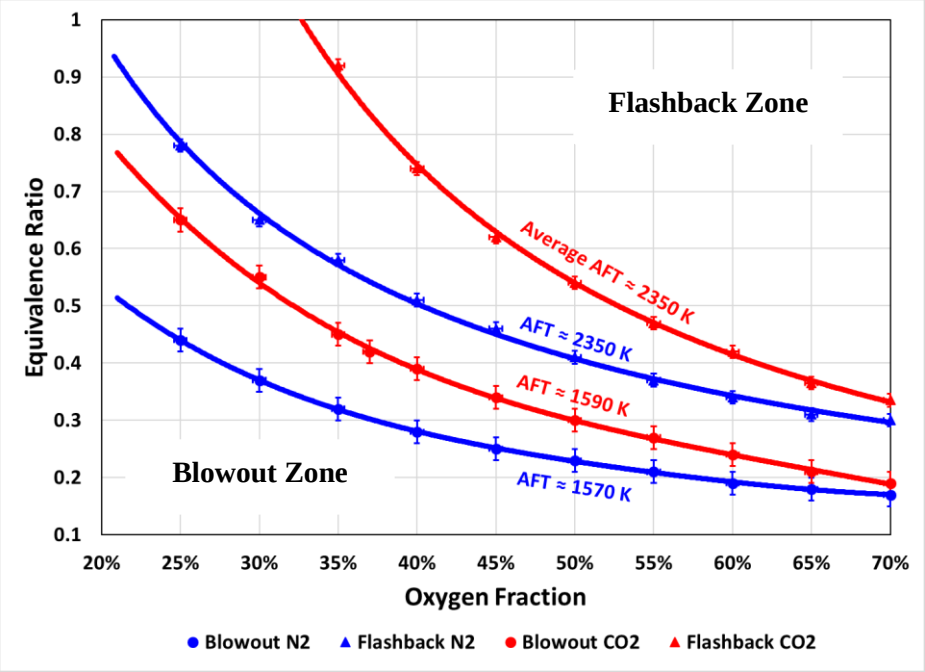


**Figure 3.3 - Comparison of the stability maps of $C_3H_8/O_2/CO_2$ and $C_3H_8/O_2/N_2$ flames.**

Some remarkable observations are:

- The blowout limits for both $CO_2$ and $N_2$ flames were reached at ~1580 K
- The flashback limits for both $CO_2$ and $N_2$ flames were reached at ~2350 K

- At the same $\varphi$, the flashback of the $N_2$ flames occurred at lower *OF* as compared to $CO_2$ flames. $CO_2$ flames have relatively retarded chemical kinetics and require more oxygen for flashback. This finding consolidates with the ones found by Jerzak and Kuźnia [77].
- The stability of $CO_2$ and $N_2$ flames start behaving identically as *OF* is increased. It is because of reduced concentrations of $CO_2$ and $N_2$ in the oxidizer mixture at higher *OF*.

These constant *AFT* contours are having distinct slopes for the blowout and flashback curves of $CO_2$ and $N_2$ flames (Figure 3.1) yet both the blowout and flashback limits of each type of flame reached at the same *AFT* (Figure 3.3). The authors have recently reported the fixed *AFT* following of the flashback limits for $CH_4/O_2/N_2$ [76] and $CH_4/O_2/CO_2$ [69] flames. The novelty of present work lies in the finding that both $C_3H_8/O_2/CO_2$ and $C_3H_8/O_2/N_2$ flames follow constant *AFT* curve not only for the flashback limit, but also for the blowout one. From these observations, it is found that the dominant role of *AFT* in controlling the chemical kinetics of the reaction is universal. For the cases of fixed inlet velocity (constant cold flow condition), the reaction kinetics mainly control the flame extinction limits. A subtle balance was observed during experiments, between flame speed and flow velocity at points of extinction. Use of constant bulk throat velocity indicates that each extinction limit is reached at a fixed flame speed. It further confirms prevailing nature of chemical kinetics in flame extinction phenomenon. Along with other parameters, the flame speed also directly depends upon the *AFT* and it becomes a reason for both types ($CO_2$ and $N_2$) of flames to extinct at constant *AFT*.

It can be inferred based on this analysis that the design and operation of premixed oxy-propane combustors are recommended to be dependent on *AFT*, notably for high and medium load configurations. This practice is also being followed in the current gas turbine markets for manufacturing the advanced LPM air-fuel gas combustors. The equivalence ratio is used for controlling the flame temperatures in air-fuel combustors, but the gas turbine manufacturers base their design, operation and evaluation of the combustors on the flame temperature (because of aforementioned reason) and not on the equivalence ratio. Constant inlet flow velocity is another common methodology in existing LPM air-fuel gas turbines and therefore the present study recommends the use of *AFT* as the controlling parameter for oxy-fuel combustors. During operations, the practice of constant pressure-drop across the combustor is maintained for achieving constant bulk throat velocity. This practice supports a safety margin for flashback event to occur in the combustor.

The flame extinction limits, in terms of blowout and flashback boundaries, of the investigated $C_3H_8/O_2/CO_2$ flames are compared in Figure 3.4 with the ones belonging to the $CH_4/O_2/CO_2$ flames obtained in a previous investigation [64] on identical combustor. It is observed that both the flashback and the blowout extinction limits of the methane flames are reached at higher $\varphi$ in contrast to those of propane flames for the same *OF* in diluted oxidizer mixture. Since *AFT* of propane is higher (roughly about 50-200 K) than that of methane for the same *OF* and $\varphi$, this difference in *AFT* shifts the stability limits of propane to lower $\varphi$, as compared to methane, for a given *OF*, because the propane flame is naturally hotter. Moreover, the blowout curves of both mixtures meet at an *OF* and $\varphi$ of about 70% and 0.2 respectively, whereas the flashback curves coincide at an *OF* and $\varphi$ of about 37% and 1.0, respectively. At these two set points, both $CO_2$ diluted oxygen-based

methane and propane flames would have, correspondingly, common blowout and flashback set points. As *OF* is higher and $\varphi$ is relatively lower in the common blowout set point, the shift between the lower stability curves of methane and propane diminishes due to leaner mixture condition. Under such lean condition, the flow rate is high enough to blowout the flame regardless the fuel type. Similarly, as *OF* is smaller and $\varphi$ is relatively larger in the common flashback point, the richer condition of the mixture contracts this shift between the two flames in the upper stability curve. Under such condition, the reactivity of the mixture is high enough resulting in flame flashback regardless of the fuel type. Further increase in equivalence ratio will convert the combustion to the rich burning zone, which is not preferred for gas turbine applications. In addition, it is observed that the propane flames have wider flame stability region than methane flames, and both zones narrow down towards larger *OF* and smaller $\varphi$. Even narrower stable flame region for oxy-propane flames than oxy-methane flames were obtained at higher *OF* and lower $\varphi$. It can be concluded that oxy-propane flames are more stable at decreased *OF* and elevated $\varphi$, whereas, oxy-methane flames are more stable at enhanced *OF* and reduced $\varphi$.

For ensuring the prominent influence of *AFT* in dictating the reaction kinetics of investigated flames, the static stability maps are mapped against curves of fixed *Re* (fFigure 3.5). The effect of difference in density of oxygen as compared to $N_2$ and $CO_2$ is evidenced in *Re* maps. The slopes of *Re* contours $[\left(\frac{\partial \varphi}{\partial OF}\right) Re]$. For the $CO_2$ map are considerably steeper as compared to $N_2$ one, demonstrating the domination of the *OF* over the oxy-fuel *Re* map, as it was previously observed with the *AFT*. The higher density of $CO_2$ attributes towards the steeper slopes of *Re* contours. Although the $N_2$ map appears to coincide with *Re* contours, no correlation is observed for $CO_2$ flames, which proves that *AFT* is the

primary controlling parameter, not *Re*. One of the previous studies of the authors [78] on coaxial non-premixed flames revealed that the structure and the stability of $CH_4/O_2/CO_2$ and $CH_4/O_2/N_2$ flames were affected with *Re* of oxidizer mixture. The *Re* maps were therefore plotted in present study for investigating the role of *Re* on flame stabilization.

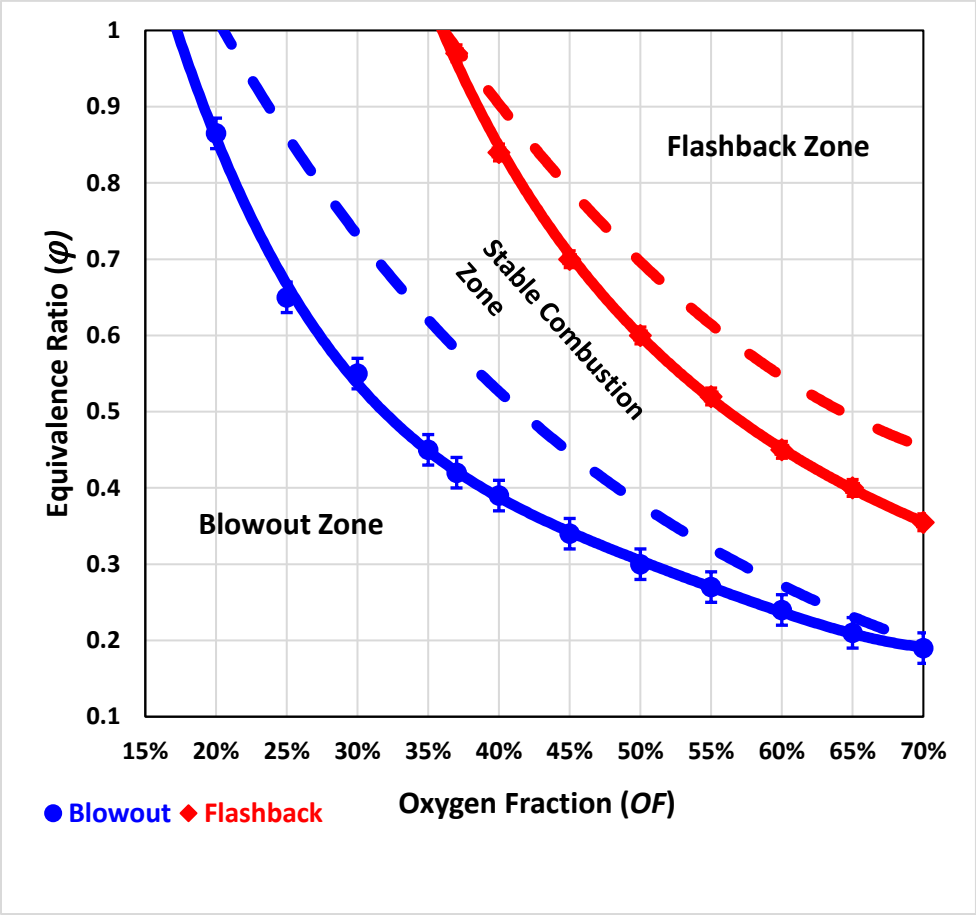


**Figure 3.4 - Comparison of static flame extinction limits of $C_3H_8/O_2/CO_2$ and $CH_4/O_2/CO_2$ flames on identical premixed swirl combustor. The dashed line curves represent the limits for the methane flames, while the solid lines represent the limits for the propane flames.**

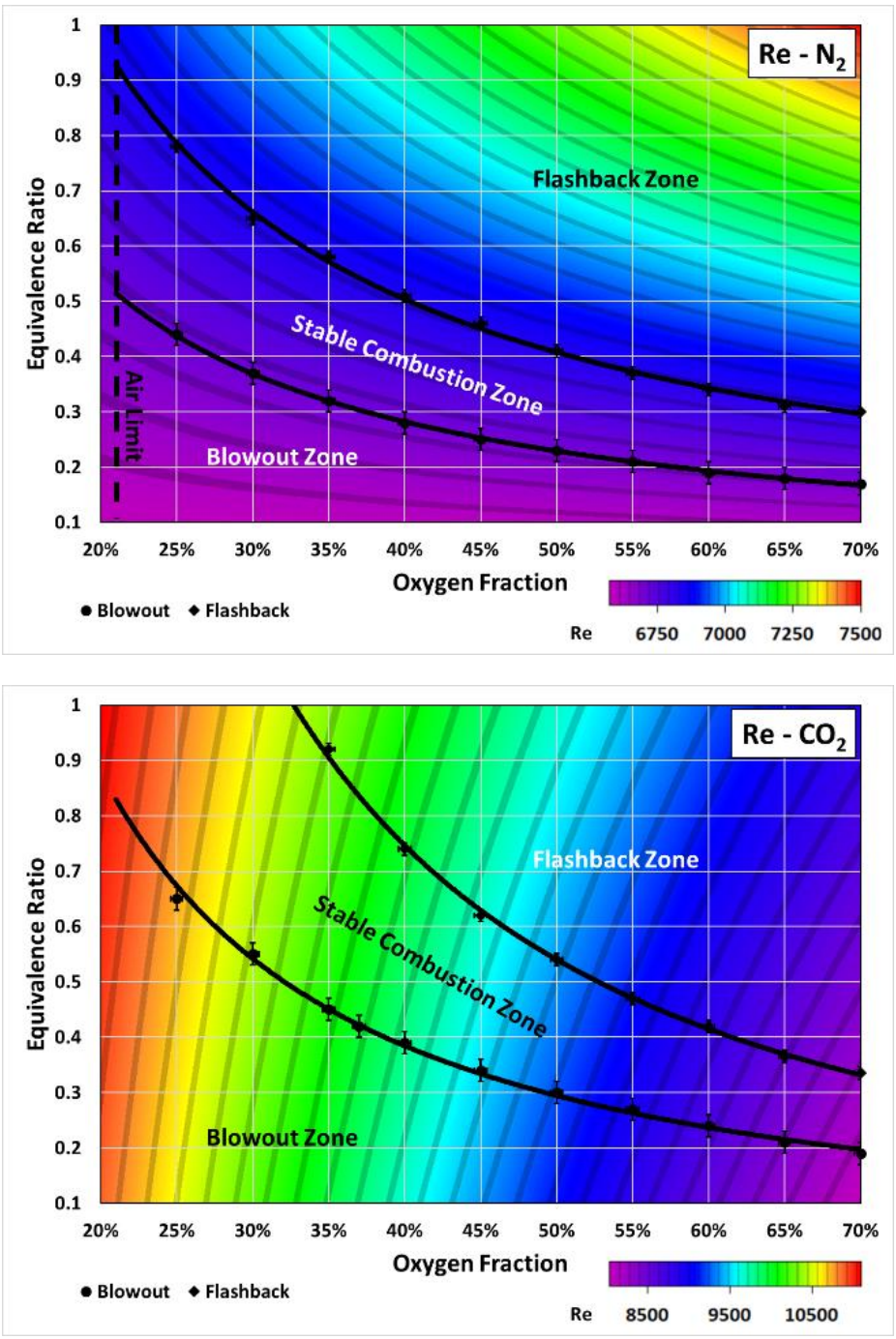


**Figure 3.5 - Static stability maps quantifying the blowout and flashback limits at constant bulk throat velocity along with constant *Re* curves for $C_3H_8/O_2/N_2$ flames (top) and $C_3H_8/O_2/CO_2$ flames (bottom).**

### 3.1.2 Flame Structure Analysis based on *AFT*

The role of *AFT* in controlling the chemical kinetics of the reaction has been discussed above in terms of flame stability. In this section, the response of *AFT* on flame structure is investigated. Figure 3.6 represents the effect of $\varphi$ on flame macrostructure at constant *OF* = 60%. As expected, increasing $\varphi$ results in increased flame strength. With the enhancement in $\varphi$, tall weak flame changes its shape to the spread-out one initially and then transitions to compact cup-shaped flame for both type of investigated flames. This shift in the flame structure is because of the increased reaction kinetics with superior $\varphi$. Despite the different $\varphi$ values in each *AFT* group, $CO_2$ and $N_2$ flames of similar *AFT* have nearly indistinguishable structures, which is a unique learning for the $C_3H_8$ flames. It validates the dominance of *AFT* in controlling the chemical kinetics of the reaction.

For further exploring the effect of constant *AFT*, different flames irrespective of the type ($N_2$ or $CO_2$), $\varphi$ and *OF* were imaged at *AFT* = 2135 K, as shown in Figure 3.7. It is observed that keeping *AFT* constant results in identical structures for both $CO_2$ and $N_2$ flames, which agrees with previous findings for $CH_4$ flames [76]. Minor changes are observed within the $CO_2$ flames because of the error associated with the simplified estimation of *AFT*; $CO_2$ flames have more effluent $CO_2$ than $N_2$ flames, as was observed in Figure 3.2. If $CO_2$ dissociation were accounted for in *AFT*, identical $CO_2$ flames would have been observed. Again, despite the significantly different $\varphi$ values at each *OF*, $CO_2$ and $N_2$ flames have nearly identical structures, because they have the same *AFT*. This finding is novel for $C_3H_8$ flames. As $CO_2$ possesses improved heat capacity as compared to $N_2$, rise in $\varphi$ of $CO_2$ flame to match *AFT* at the same *OF* is just a penalty to be paid to overcome its higher heat capacity.

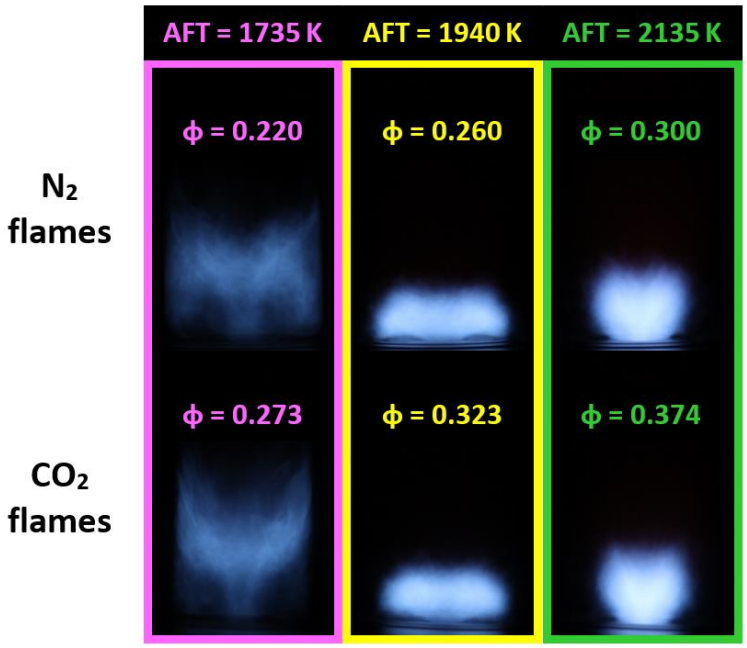


**Figure 3.6 - Effect of $\varphi$ on flame structure at constant *OF* = 60%**

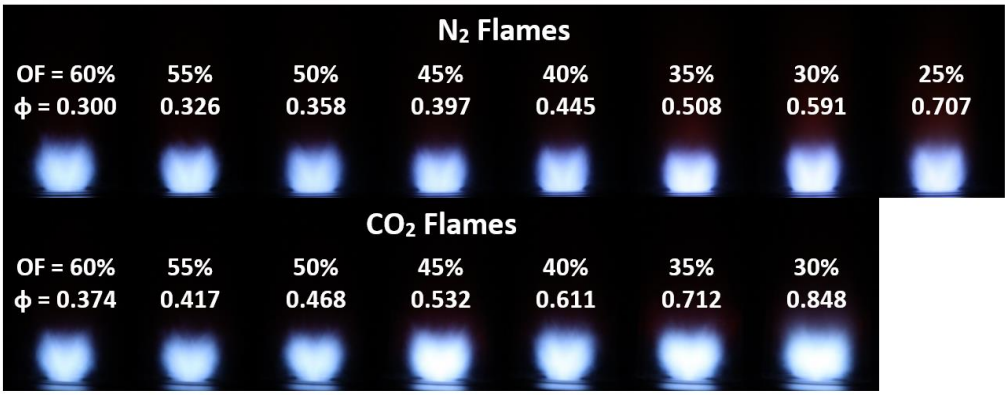


**Figure 3.7 - Effect of maintaining constant *AFT* on flame structure. All $CO_2$ and $N_2$ flames have *AFT* = 2135 K**

Flame images pertaining to the similar $\varphi$ and *OF* but different *AFT* are also captured, as shown in Figure 3.8. It is noticed that switching from $N_2$ to $CO_2$ reduces the *AFT*, as expected, due to superior heat capacity of $CO_2$. In addition to the negative impact of $CO_2$ on reaction kinetics, The lower *AFT* results in deteriorated flame strength. This figure (i.e.

Figure 3.8) plus the two previous figures (i.e. Figure 3.6 and Figure 3.7) prove that *AFT* plays a decisive role in controlling flame structure. Matching $\varphi$ or *OF* does not result in identical flames but matching *AFT* does, which is the novel finding of the presented study.

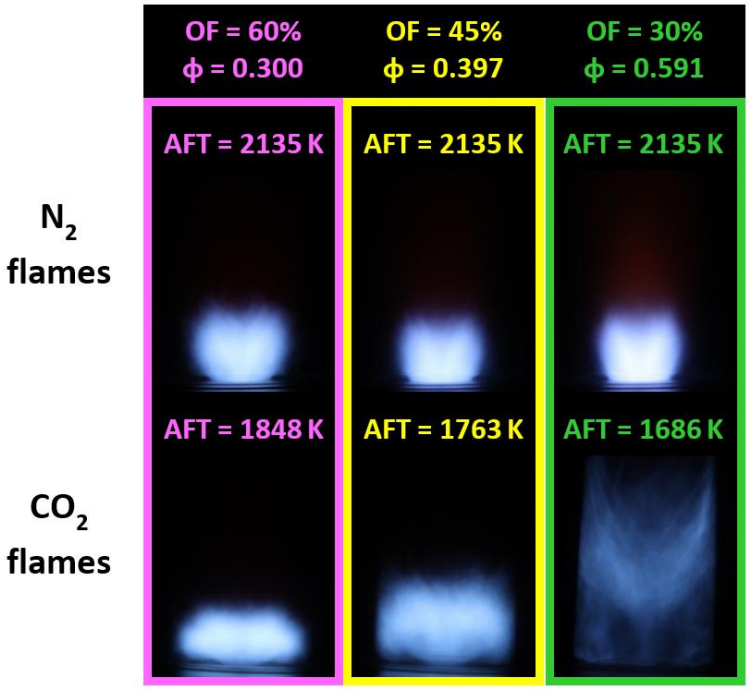


**Figure 3.8 - $N_2$ and $CO_2$ flames of the identical *OF* and $\varphi$ but different *AFT***

For further analyzing the flame macrostructure and stabilization, flame images are captured as $\varphi$ is reduced at a fixed *OF*, from near flashback extinction limit to the vicinity of blowout one. The value of $\varphi$ is noted as flame macrostructure significantly changes. These notable $\varphi$ values are then indicated on the stability maps of $CO_2$ and $N_2$ flames (Figure 3.9). Near the flashback region, the flames (red-bordered) are compact, indicating higher reaction kinetics and dominance of inner recirculation zone (*IRZ*). As $\varphi$ value is decreased, the flame spreads out (yellow-bordered). A further bit of drop in $\varphi$ results in the flame starting to lift-up from the base of the combustor (green-bordered). The outer recirculation zone

(*ORZ*) starts to compete with *IRZ* thus resulting in flame lift-up. With further reduction in $\varphi$, the macrostructure of the flame finally transitions itself into a conical shape (blue-bordered), indicating the dominance of *ORZ* on the flame structure. In transition of flame macrostructure from compact flames to tall conical ones, reduction in flame noise is also observed during the experiments. Furthermore, with lower *OF* in $CO_2$ flames, the transition from red-bordered flame to the yellow-bordered one resulted after substantially decreasing the $\varphi$ value. It is because of elevated heat capacity possessing $CO_2$ concentrations at reduced *OF*. Moreover, *AFT* of each macrostructure for $CO_2$ flame is higher as compared to $N_2$ flame, also due to elevated heat capacity of $CO_2$.

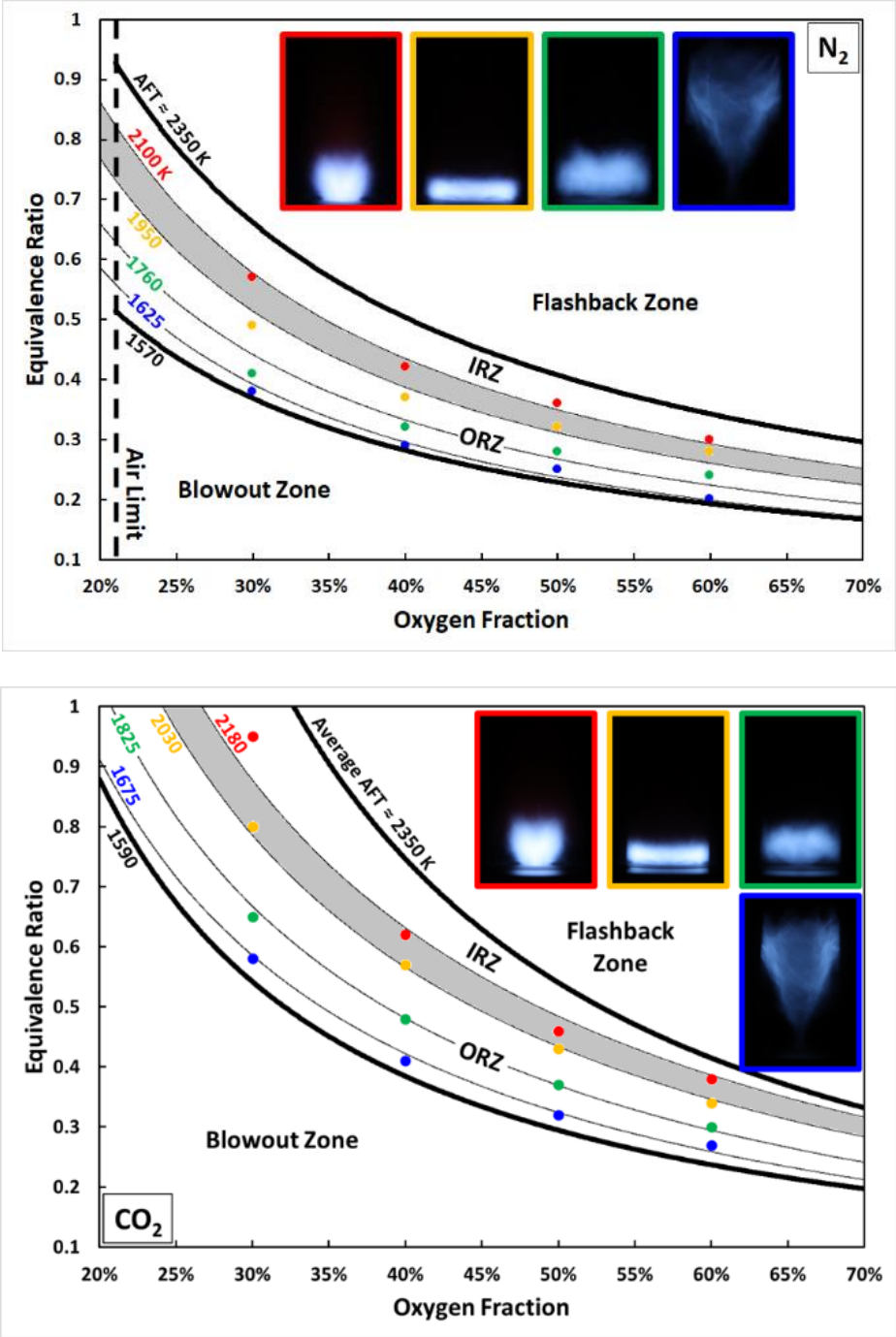


**Figure 3.9 - Transition from *IRZ* to *ORZ* stabilization in $N_2$ (top) and $CO_2$ (bottom) flames.**

The outcomes of this investigation trigger the recommendation of designing and operating the prospective combustor of oxy-propane gas turbine dependent on *AFT* and not dilution

ratio or percent exhaust recirculation. *AFT* can easily be estimated for any given set of operating conditions. The stabilization modes and shapes of the stable oxy-propane flames may be clearly deduced based on the information of *AFT* alone. Thus, it is recommended to design the heat shields of combustor headend to be based on *AFT* and its information is also useful in predicting the interaction of adjacent flames, along with the resulting instabilities, in the multi-premixed combustors.

### 4.1.3 Characterization of Flame Temperature

At different locations, the temperature of $C_3H_8/O_2/CO_2$ flames was measured inside the quartz confinement to further explore the relationship between *AFT* and flame structure. For oxy-fuel combustion conditions, the flame temperature measurements may aid the validation of numerical models. Table 4.1 refers the operating conditions of flames A and B for which local mean temperatures were measured, whereas Figure 3.10 displays their respective flame shapes. The temperature measurements were performed in reference to the axial distance, *Z* (cm). A bottom reference value of $Z = 0$ cm was assigned to the base of quartz confinement i.e. the exit plane of the burner divergent section and a top value of $Z = 30$ cm was allocated to the exit plane of the quartz confinement. Figure 3.11 represents centerline axial temperature distribution of selected flames from above the flame structure, $Z = 10$ cm to $Z = 21$ cm. Since both flames are having nearly similar *AFT* value, the temperature profiles of both flames also show similar trends. It should also be noted from Table 4.1 that although *AFT* of both flames is nearly equal but the combination of $\varphi$ and *OF* is quite different. Figure 3.11 also shows that the measured temperatures are slightly different from the theoretical *AFT*, with flame B having a bit higher temperature than flame A at every axial location. It was noticed while testing different flames that the noise coming

out of the quartz tube gets stronger as *AFT* of the flame increases. Figure 3.10 shows that flame shape is strongly dependent on *AFT*, as flames A and B present similar plume shape. As $\varphi$ and *OF* conditions of both flames are quite different but because of similar *AFT* only, the flame shapes become similar. Such findings reinforce the role of *AFT* as the main controlling parameter of flame structure and stability.

**Table 4.1:** Test conditions of temperature measurements.

| Flame number | *OF* | $\varphi$ | *AFT* (K) |
|---|---|---|---|
| A | 60% | 0.39 | 2195 |
| B | 30% | 0.89 | 2202 |

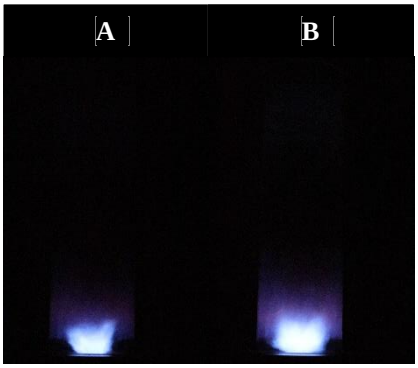


**Figure 3.10 - Flame images as listed in Table 4.1**

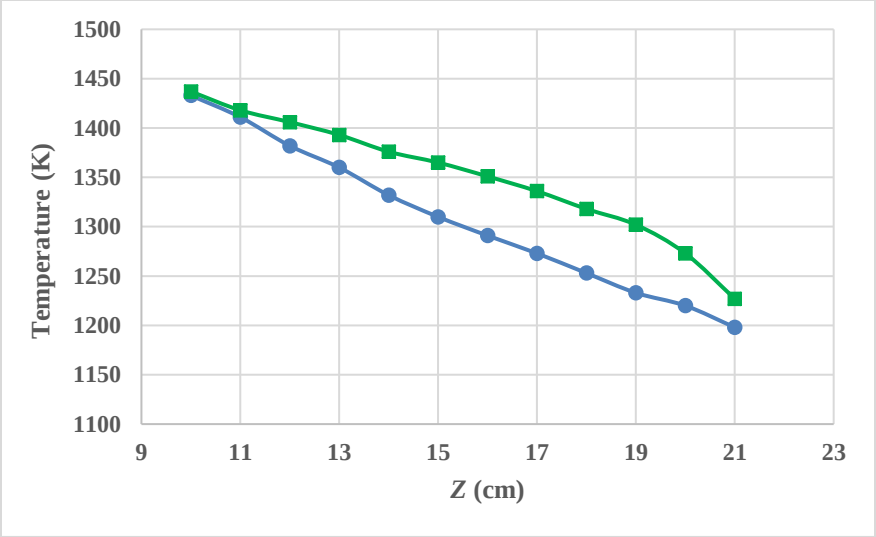


**Figure 3.11 - Axial centerline temperature distributions for flames A (circular data points) and B (rectangular data points), with *Z* = 0 cm representing the base of the combustor**

Due to combustion dynamics, flames cannot be considered as slug flow reactors. Therefore, the radial temperature profiles of the different flames were also measured at two axial locations, $Z$ = 21 cm and $Z$ = 10 cm, and the outcomes are illustrated for better understanding of the flame structure in Figure 3.12 and Figure 3.13, respectively. Both the flames show decreasing temperatures at locations radially away from the plume. The temperatures shown in Figure 3.12, axially away from the flame, are lower than those in the vicinity of the flame core as displayed in Figure 3.13. The temperature profiles in two figures infer the two-dimensional nature of the flow field. Because of the existence of an inner recirculation zone (*IRZ*), the maximum temperatures values are not located at the centerline of the combustor. Figure 3.12 indicates maximum temperature at a radial distance of 0.5-1.0 cm, while Figure 3.13 reports it at radial distance of 1.0-1.5 cm. The difference here indicates the presence of local *IRZ* of relatively larger size in near exit location of the burner and then gradually decreasing towards the downstream along axial

direction. This recirculation zone is more dominant and thus visible in weaker flames (see $CO_2$ and $N_2$ flames at *AFT* = 1735 K in Figure 3.6) as compared to the stronger ones.

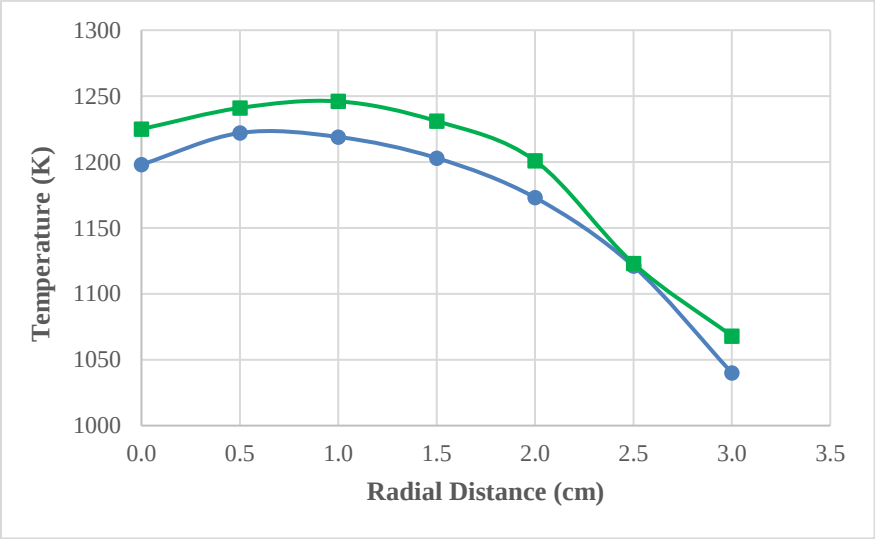


**Figure 3.12 - Radial temperature distributions for flames A (circular data points) and B (rectangular data points) at Z = 21 cm**

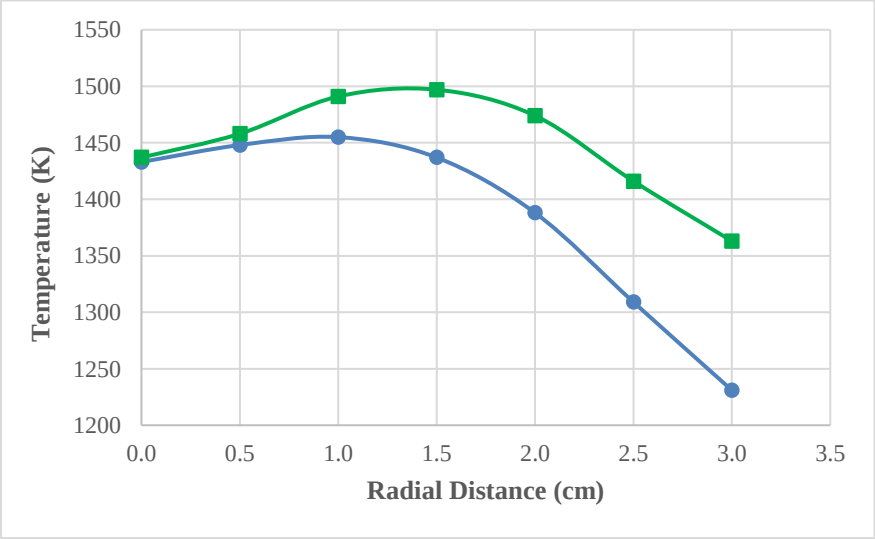


**Figure 3.13 - Radial temperature distributions for flames A (circular data points) and B (rectangular data points) at Z = 10 cm**

## 4.2 Simulation Results of $CH_4/H_2/O_2/CO_2$ flames

### 4.2.1 Structure and Stability of $CH_4/H_2/O_2/CO_2$ flames

Flame shape visualization is an important part of analysis for harnessing thorough understanding of flame characteristics. The assessment of different flame shapes also provides insight on flame extinction mechanisms. Figure 3.14 compares natural luminosity images with the numerically generated flame shapes represented as the contours of OH radicals.

Figure 3.14a considers the effect of varying *HF* on the flame shape. For smaller fractions of hydrogen (*HF*=40%) in the fuel mixture, flame possesses a spread-out shape, while for higher hydrogen fractions (*HF*=60%), flame becomes compact and perturbed indicating improved reactivity of the mixture with hydrogen-enrichment. This finding is in agreement with previous investigations reporting enhanced laminar flame speeds as a result of hydrogen-enrichment [79,80]. Higher OH concentrations are observed in numerical flame shape with increasing hydrogen fraction (*HF*=60%), indicating improved reactivity of the mixture. The dark zone below the flame and besides the burner wall in the experimental flame shapes is a representation of the quenching effect. In the *ORZ*, no reaction occurs and there is also some cooling effect near the wall, resulting in local quenching.

Figure 3.14b reveals the consequence of varying *OF* on flame shape. Experimental images indicate brighter and compact flame with increased *OF*, signifying the enhanced reactivity of the combustible mixture due to oxygen-enrichment. The availability of more oxidizer to the fuel results in greater concentrations of reactive species, thus accelerating the chemistry. Similarly, the numerical flame shapes also show that the OH concentration

increases significantly at higher fractions of oxygen (*OF* =38%) in the oxidizer mixture. Figure 3.14c explores the effect of bulk throat velocity on the reactivity of combustible mixture by analyzing the flame shape. It is observed that low bulk velocities ($U_{in}$=4.4 m/s) result in strong flame as compared to the higher bulk velocity ($U_{in}$=6.0 m/s). It can be ascribed to consequent increase in residence time for the radicals to interact and react with other chemical species, and thus leading to relatively complete combustion at reduced bulk velocity. Numerical flame shapes also confirm this effect by exhibiting higher OH concentration at reduced velocity. In all the three comparisons shown in Figure 3.14, numerical findings are in agreement with experimental flame shapes, which validates the numerical code used for these simulations.

In order to study flow-flame interactions in the current test cases, the numerical data is further explored by mapping the velocity vectors over static temperature contours as shown in Figure 3.15. The creation of both outer recirculation zone (*ORZ)* and inner recirculation zone (*IRZ*) characterizes overall features of turbulent reacting flow field. Figure 3.15a compares the influence of *HF* on the temperature and flow fields. At lower hydrogen fraction (*HF*=40%), a large primary eddy (*PE*) is observed in the downstream (centered at Z/D=0.6) preceded by a small recirculation zone slightly upstream of it indicating an impending smaller secondary eddy (*SE*). With increasing hydrogen concentrations (*HF*=60%), *PE* is formed rotating clockwise in the downstream (centered at Z/D=0.2) while two *SEs* are created upstream of it, rotating in opposite direction to each other. The creation of eddies enhances the turbulent-induced mixing, and thus improves the flow reactivity.

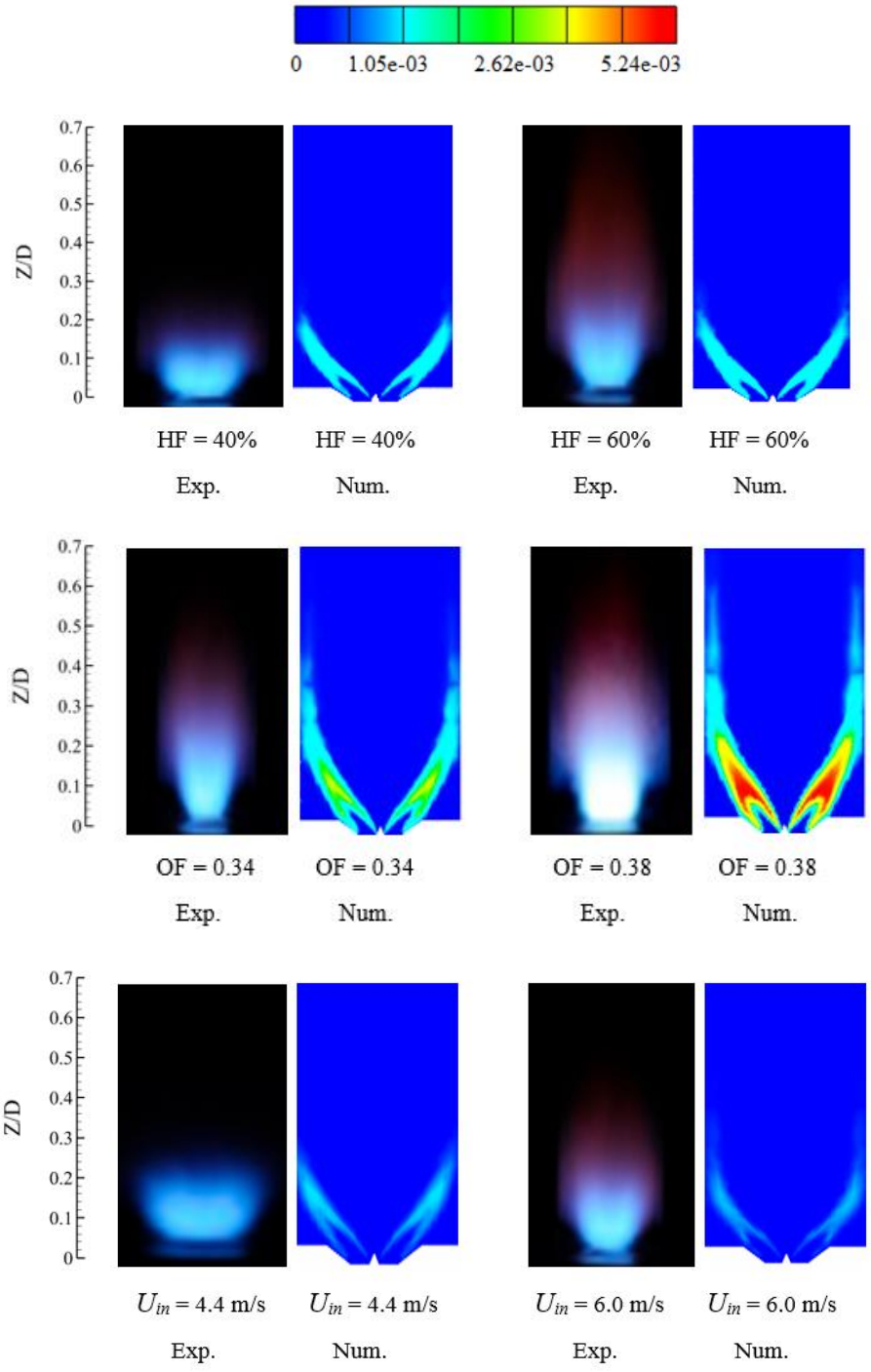


**Figure 3.14 - Experimental (images taken with high-speed camera) and numerical (OH contour plots) flame structure comparison under stoichiometric condition at varying: hydrogen fractions at $U_{in}$=5.2 m/s (top), oxygen fractions at $U_{in}$=5.2 m/s (middle), and bulk throat velocities at *HF*=20% and *OF*=30% (bottom)**

Figure 3.15b indicates the role of the *OF* on thermal structure of flame. Increasing *OF* results in elevated temperatures because of the enhanced availability of O radicals in the combustible mixture. The temperature, for all cases, approaches about 2300 K in the upstream region but at the combustor exit it scales back to normal values, which is appropriate and reliable for the operations of turbine blades. This interaction of radicals with combustible mixture further enhances reactivity as several eddies are formed. At lower oxygen concentration (*OF*=34%), a *PE* appears to be rotating counterclockwise, followed by the opposite direction rotation of a *SE*. Far upstream, another smaller *SE* can be seen rotating in the clockwise direction. At *OF*=38%, the secondary eddies breakdown into several smaller counter-rotating eddies towards downstream, indicating enhanced flame-vortex interactions driven by turbulence-induced coarse mixing. Overall, increasing hydrogen and/or oxygen concentration enhances the reaction rates and thus results in strong and compact flames, as also witnessed in experimental flame shapes as shown in Figure 3.14a and Figure 3.14b.

Figure 3.15c represents physical effects of the bulk throat velocity on the reactant mixture. At lower inlet velocity ($U_{in}$=4.4 m/s), reactant species get more residence time to react with each other [81] and one *PE* and one *SE* are formed, both rotating in opposite directions. Whereas, at enhanced inlet velocity ($U_{in}$=6.0 m/s), only one *PE* is observed rotating in the counterclockwise direction, indicating reduced reactivity of the mixture. In all the three cases of varying *HF*, *OF*, and $U_{in}$, a smaller *ORZ* is formed at the bottom corner of the reactor, which largely remains unaffected most probably due to its farther location from the flame. Suliman et al. [29] carried out experiments for investigating the flame stability at bulk throat velocity of 6.0 m/s. They have reported flame static stability map versus the

curves of fixed *AFT*, as shown in Figure 3.16. The temperatures indicated by the simulation of the present study are also validated from his experimental work, as stable flame with *HF*=20%, *OF*=30% and $U_{in}$=6.0 m/s possesses maximum temperature of about 2400 K for both the results reported by Suliman et al. [29] and the present study.

Vorticity is an adequate representation of the tendency of rotation of the flow field which is also directly related to the formation of turbulent eddies. Figure 3.17 represents the magnitude of vorticity contours for different mixture compositions. The region between the inner and outer shear layers indicate dominant reaction zone in the form of stabilized flame. The inner shear layer thickens up with increase in *HF*, as shown in Figure 3.17a. It is because of the higher vorticity levels in the vicinity of the center of the combustor. Similarly, vorticity increases with increasing *OF* with increased inner shear layer thickness (Figure 3.17b). Vorticity has high magnitude with increased bulk throat velocity case, as shown in Figure 3.17c, but the length of the inner and the outer shear layers decreases with augmentation in the bulk throat velocity. The dominance of *ORZ* owing to increased velocity ($U_{in}$ =6.0 m/s) might be its possible reason, at which the outer shear layer extends itself and flame, therefore, stabilizes at the corner region of the combustor.

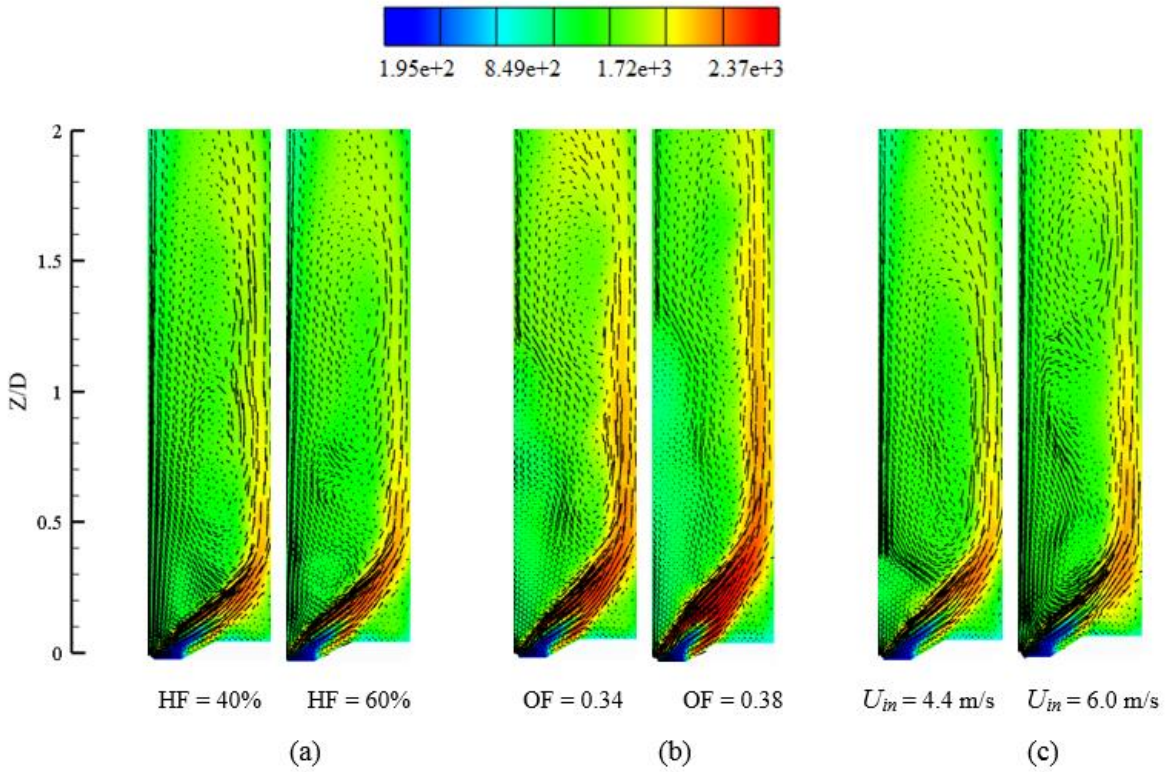


**Figure 3.15 - Calculated velocity vectors mapped over temperature (in kelvins) contours under stoichiometric condition with varying: (a) hydrogen fractions at $U_{in}$=5.2 m/s, (b) oxygen fractions at $U_{in}$=5.2 m/s, and (c) bulk throat velocities at *HF*=20% and *OF*=30%**

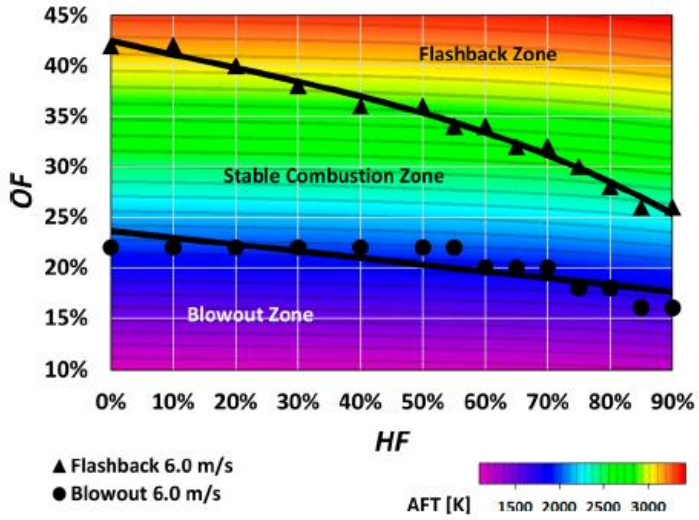


**Figure 3.16 - Stability map quantified with blowout and flashback limits at $U_{in}$=6.0 m/s [29]**

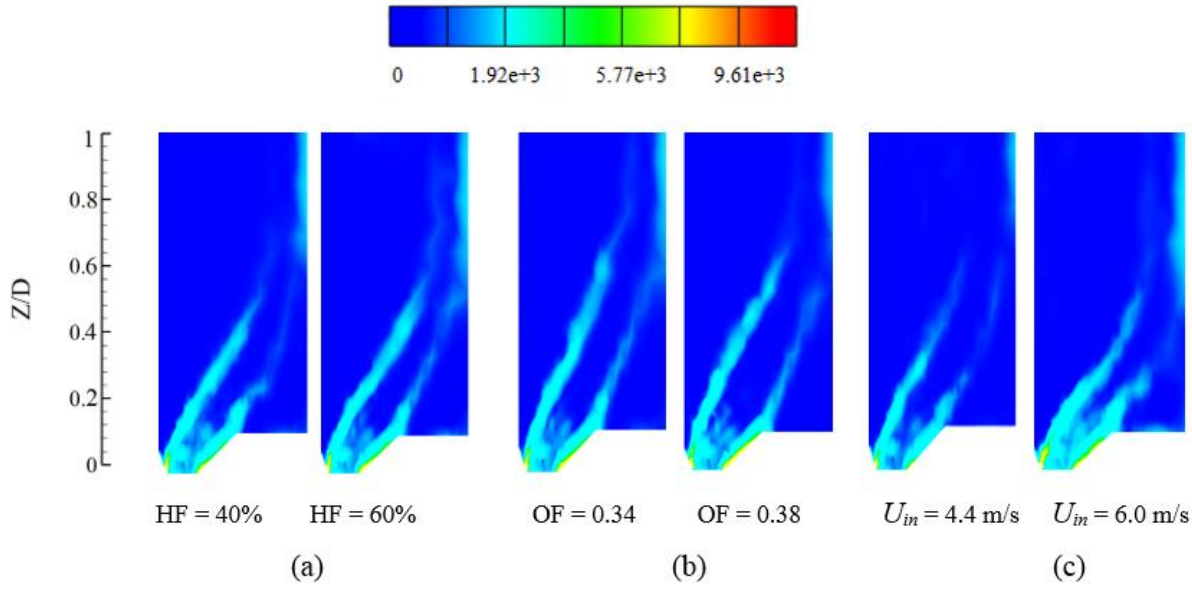


**Figure 3.17 - Calculated contours of vorticity (1/s) under stoichiometric condition with varying: (a) hydrogen fractions at $U_{in}$=5.2 m/s, (b) oxygen fractions at $U_{in}$=5.2 m/s, and (c) bulk throat velocities at *HF*=20% and *OF*=30%**

### 4.2.2 Combustion and Emission Attributes of $CH_4/H_2/O_2/CO_2$ flames

Hydrogen-enriched premixed flames characteristics are analyzed by investigating the product formation rate (*PFR*). Figure 3.18 shows the effect of *HF*, *OF*, and bulk throat velocity $U_{in}$ on the product formation rate (*PFR)* – an important combustion parameter. With hydrogen (Figure 3.18a) and/or oxygen (Figure 3.18b) addition, the *PFR* in relatively thin inner shear layer increases, resulting in compact flames. The influence of the *OF* on *PFR*, however, is comparatively greater than that of HF. At lower bulk throat velocity, on the other hand, *PFR* in the inner shear layer increases resulting in shorter flame structure (Figure 3.18c). The effect of inlet velocity on *PFR*, however, is small which implies that chemical aspects of the flame dominate compared to its physical features in terms of the rate of product formation. The numerical model does not capture the stability transition of

the flames from the ORZ to the IRZ, but the trend of *PFR* sheds light on it. Flame images from Figure 3.14 can be recalled for corner flame stabilization at lower *HF* and *OF*, and high $U_{in}$ indicating the dominant role of the *ORZ* on flame stability; however, its role diminishes with increasing *HF* and *OF*, and lowering $U_{in}$.

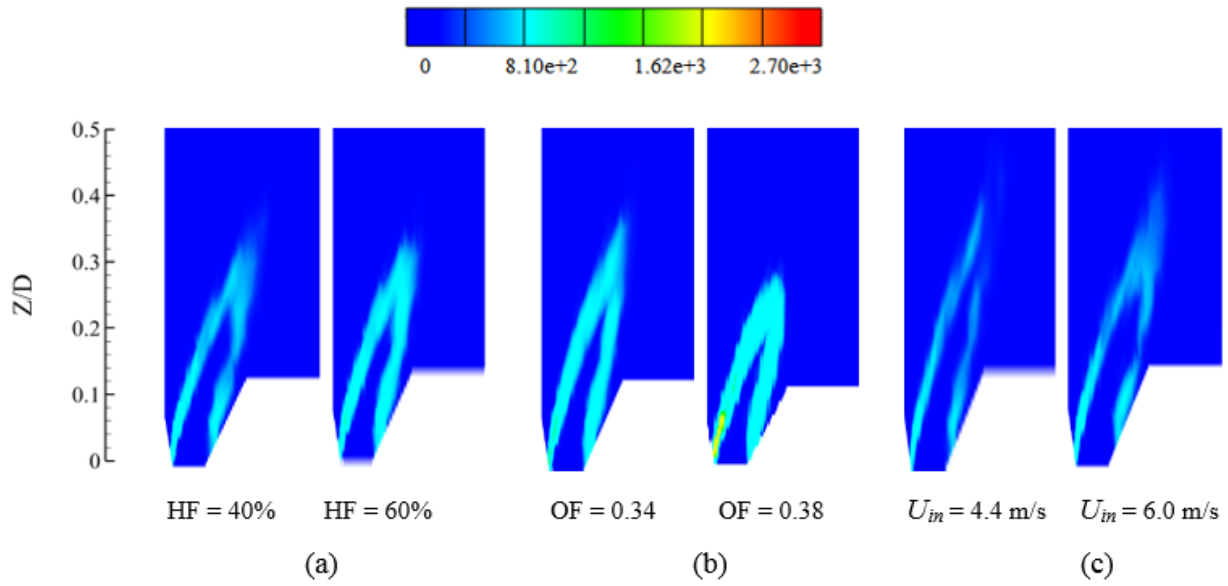


**Figure 3.18 - Calculated contours of product formation rate (1/s) under stoichiometric condition with varying: (a) hydrogen fractions at $U_{in}$=5.2 m/s, (b) oxygen fractions at $U_{in}$=5.2 m/s, and (c) bulk throat velocities at *HF*=20% and *OF*=30%**

Another important parameter is reaction progress variable *c* for characterizing flame structure, and for indicating the degree of completion of the combustion reaction by showing conversion from unburnt reactants to entirely burnt products (complete combustion). The contours of progress variable in Figure 3.19 represent the influence of *HF*, *OF*, and throat velocity on the progress of the reaction. The individual impact of increased oxygen- and hydrogen-enrichment on the progress variable do not seem to be significant as the figure hardly show any differences particularly in the near-exit location

of the burner where the flame stabilizes. Similarly, the increase in bulk throat velocity also does not make any difference to the flame thickness (represented by progress variable) even though the resulting increase in angular momentum dislocate the flame-front by pushing it outwards. It is also worthy to note here that the resulting increase in turbulence hardly affect the flame thickness, suggesting the dominant role of chemical kinetics which remains unaffected by the flow dynamics.

For analyzing the emissions characteristics of the flames under investigation, mole fraction distributions of CO, OH, $CO_2$ and $H_2O$ species are studied (Figure 3.20). The results of hydrogen-enrichment are witnessed with increased CO and reduced $CO_2$ concentrations. One of the possible reasons is the increment in *HF* makes more H species available, which compete with CO for its reaction with atomic O; thereby retarding $CO_2$ and increasing OH formation. Atomic O and H tend to react at first hand, as compared to the CO oxidation to $CO_2$. In addition, increasing *HF* results in increased combustor temperatures for the premixed stoichiometric oxy-methane flames, which consequently becomes a reason for the $CO_2$ dissociation into CO and O species. This phenomenon would have dominated and resulted in the increased CO concentrations. Furthermore, the availability of more H species due to hydrogen-enrichment, increases the formation of $H_2O$ through OH.

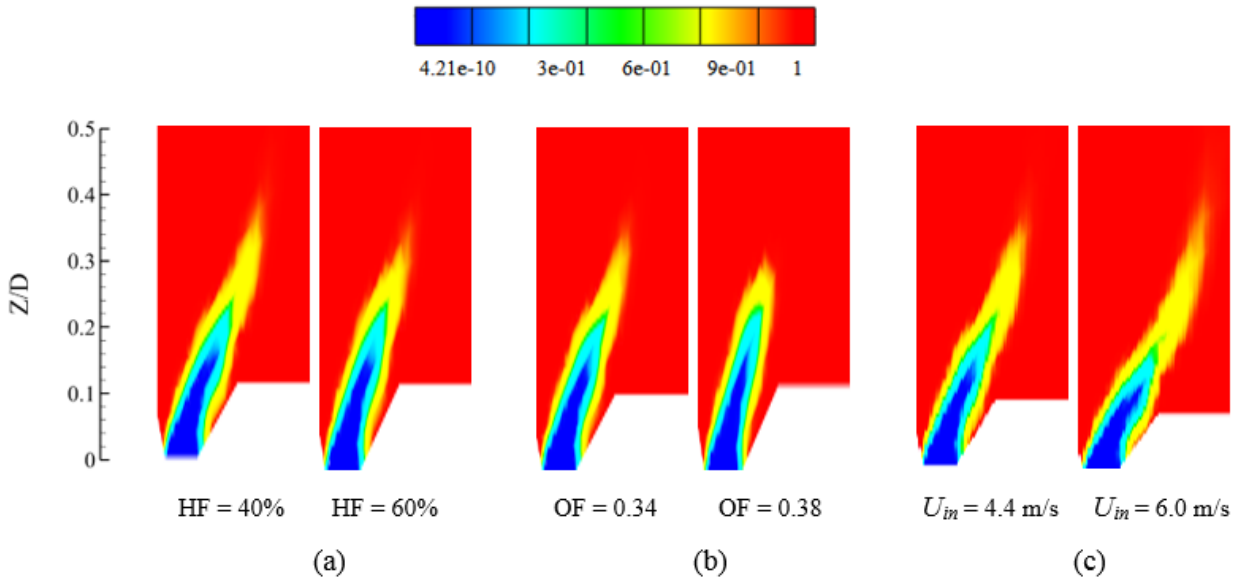


**Figure 3.19 - Calculated contours of progress variable under stoichiometric condition with varying: (a) hydrogen fractions at $U_{in}$=5.2 m/s, (b) oxygen fractions at $U_{in}$=5.2 m/s, and (c) bulk throat velocities at *HF*=20% and *OF*=30%**

The mole fraction of CO and OH species increases with rising *OF*. The availability of increased concentrations of $O_2$ makes the possible break down of $CH_4$ and $H_2$ molecules and oxidation results in CO and OH species. $CO_2$ is one of the complete combustion products but also, it is part of the reactant oxidizer mixture. On one side, CO is oxidizing to $CO_2$ but because of the elevated temperatures, the breaking effect of $CO_2$ into CO and O species prevails and therefore increasing *OF* would have resulted in increased CO while reduced $CO_2$ concentrations. In addition, increasing the *OF* enhances OH oxidation and therefore results in increased concentrations of $H_2O$.

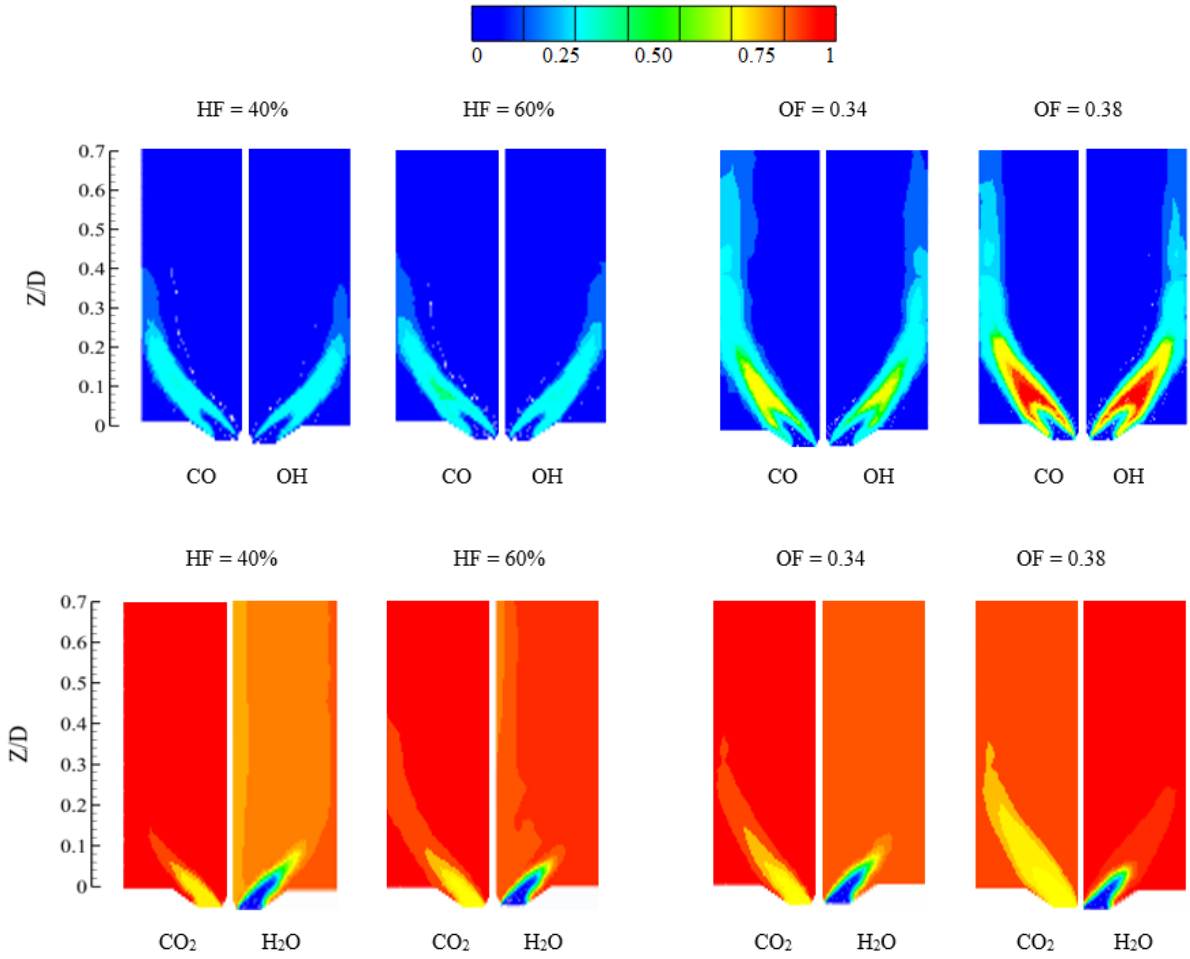


**Figure 3.20 - Calculated dimensionless mole fractions of CO, OH, $CO_2$, and $H_2O$ distributions under stoichiometric condition with varying hydrogen and oxygen fractions**

Figure 3.21 shows the behavior of hydrogen fraction, oxygen fraction, and inlet velocity affecting the total thickness of the flame ($\delta$ = preheat zone + reaction zone) ($\delta = \pi\ (\delta)$). Augmenting the concentrations of hydrogen and oxygen gases further make the flame thinner as indicated in Figure 3.21a and Figure 3.21b, respectively. It is worthy to mention that reduction of flame thickness is more severe with increasing *OF* as compared to *HF*. Bulk throat velocity is the physical property of the mixture and, therefore, it puts negligible effect on flame thickness. Figure 3.22 represents the changes in Damköhler number (*Da*) with *HF*, *OF*, and $U_{in}$. The *Da* significantly enhances with the increments in hydrogen and

oxygen, witnessed in Figure 3.22a and Figure 3.22b, indicating faster reaction with more addition of each gas. Moreover, the increase of the inlet velocity results in reduction of the *Da* (Figure 3.22c), because transport time scale overwhelms chemical time scale relatively as a consequence of reduced residence time. Furthermore, value of *Da* is more than unity for all investigated cases, representing influential role of chemical kinetics on flame characteristics. The flame structure is thin and increased value of *Da* indicates the prominent part of laminar burning rate, while turbulence does not alter the inner structure of the flame because of thinner flames and disturbs the overall outer structure of the flame. That seems to be the reason behind wrinkled and spread-out flames.

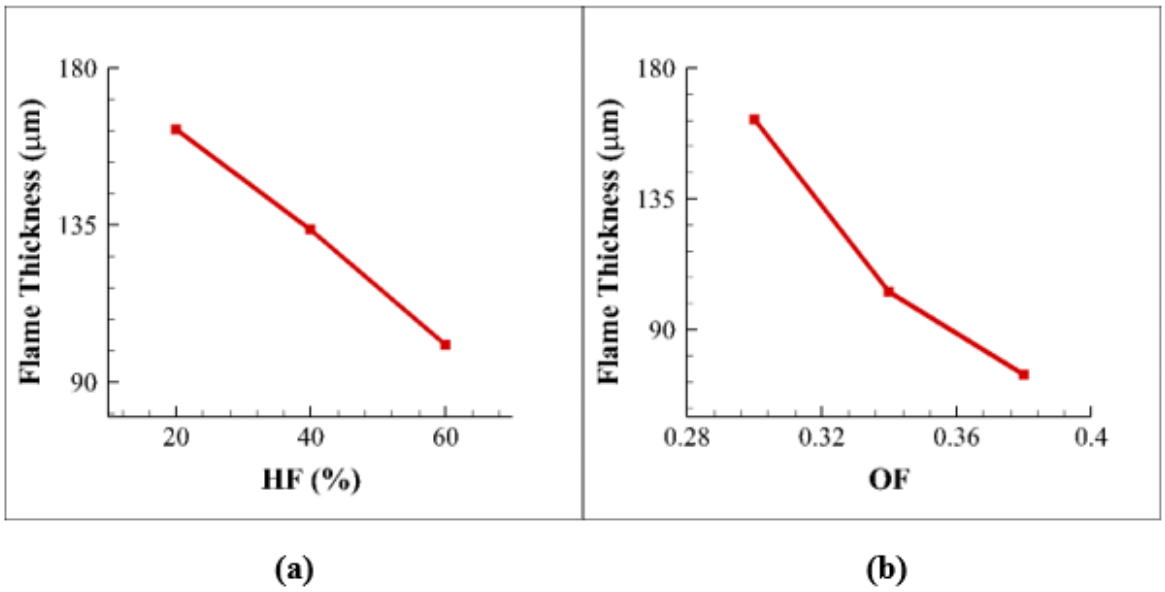


**Figure 3.21 - Effects of: (a) hydrogen fraction and (b) oxygen fraction (both at $U_{in}$=5.2 m/s and *OF*=30%) on calculated flame thickness under stoichiometric condition**

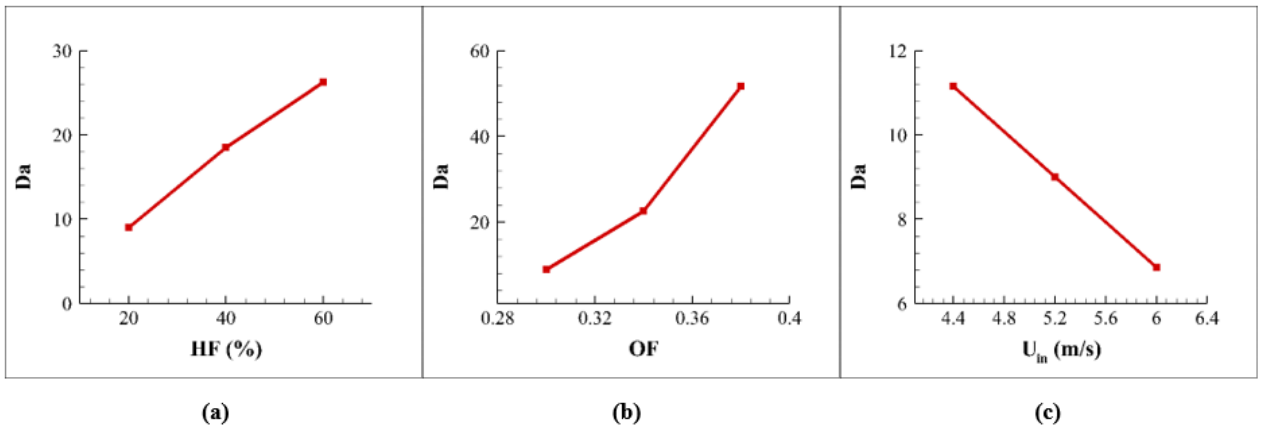


**Figure 3.22 - Variation of calculated Damköhler number (*Da*) under stoichiometric condition as function of: (a) hydrogen fraction at *OF*=30% and $U_{in}$=5.2 m/s, (b) oxygen fraction at *OF*=30% and $U_{in}$=5.2 m/s, and (c) bulk throat velocity at *HF*=20% and *OF*=30%**

# CHAPTER 5

# CONCLUSIONS

The stability and combustion characteristics of oxy-propane ones ($C_3H_8/O_2/CO_2$) and oxygen-enriched air-propane flames ($C_3H_8/O_2/N_2$) were analysed and compared using a model gas turbine combustor, under identical conditions of oxygen fraction (*OF* = 21% - 70%) and equivalence ratio ($\varphi$ = 0.1 - 1.0). Operational air-fuel gas turbine combustor's geometry was mimicked by the investigated swirl-stabilized combustor implementing LPM DLE technology. Throughout the study, the flow rates of the non-preheated reactant gases were adjusted for establishing a common inlet velocity of 5.2 m/s and for maintaining similar turbulence intensities and flow conditions. The enrichment of atmospheric air with pure oxygen was used for the production of artificial air ($O_2/N_2$) of specific *OF*. The stability map of the combustor was plotted based on quantification of the blowout and flashback flame extinction limits within $\varphi$-*OF* domain. Adiabatic flame temperature (*AFT*) was mapped over the same test ranges for both $CO_2$ and $N_2$ flames. In addition, the behavior of constant *AFT* was investigated in detail, over the flames' macrostructure and stabilization by imaging selected flames. For the common bulk throat velocity of $N_2$ and $CO_2$ flames, the subsequent novel conclusions were identified. (a) The constant *AFT* contours were distinct of individual flames, yet their stabilization zones can be clearly characterized by *AFT* alone. Thus, under similar flow conditions, the reaction kinetics primarily govern the stable combustion zones. (b) While increasing the *AFT* of both $CO_2$ and $N_2$ flames from blowout to flashback limit, similar changes occur in the macrostructure

and stabilization mode. (c) Flames with similar *AFT* possess similar flame shape, even though the *OF* and $\varphi$ are different, which proves the dominance of reaction kinetics in the behavior of flames. It also demonstrates that the information of *AFT* alone is useful enough to accurately predict the macrostructure and stability of $CO_2$ and $N_2$ flames with constant bulk throat velocity. Axial and radial temperatures were measured inside the quartz confinement for investigating the field of flow. Based on the prevailed findings, this thesis work proposes the design and operation of prospective oxy-propane gas turbines founded on *AFT* (and not on $\varphi$ or *OF*).

Moreover, Stoichiometric premixed $CH_4/H_2/O_2/CO_2$ flames are numerically simulated incorporating Large Eddy Simulations (LES) for investigating effects of hydrogen-enrichment (*HF*), oxygen fraction (*OF*), and bulk throat velocity ($U_{in}$) on flame characteristics and stability, as well as the resulting emissions. Three constant velocities were investigated in this analysis i.e. 4.4 m/s, 5.2 m/s and 6.0 m/s. The outer recirculation zone (ORZ) plays a significant part in flame stabilization at lower values of *HF* and *OF*, but its role diminishes at higher values. The inner recirculation zone (*IRZ*) is mainly characterized with the formation of secondary eddies whose number and size strongly depends upon the *HF* and *OF* of the mixture.

The rate of reaction increases significantly with increasing *HF* and *OF*, because of the increased concentrations of chemically active radicals. The concentration of CO enhances whereas the mole fraction of $CO_2$ reduces with increasing *HF*. Elevated temperatures trigger the $CO_2$ dissociation into CO and O atoms. In addition, increased OH species are noticed because of the availability of more H species. $CO_2$ also reduces down with increasing CO emissions at higher *OF*. The accessibility of more O atoms to CO would

cause improved oxidation to $CO_2$ however, the dissociation of $CO_2$ because of higher temperatures, prevails its formation. With increasing *HF* and *OF*, the Damköhler number (*Da*) boosts and reduces down with increments in the bulk throat velocity. The higher values of *Da* suggest that, although the swirl-generated turbulence slightly affects the macrostructure of the flame, the flame's compositional structure is governed by the overall stoichiometry such that the propagation reactions dominate the flame-front region and keep its micro-structure largely intact.

# CHAPTER 6

# FUTURE WORK

- The premixed $C_3H_8/O_2/N_2$ and $C_3H_8/O_2/CO_2$ flames can be numerically studied for further insight on the attributes of efficient combustion and reduced emission operations.
- This combustor can be used for conducting experiments with biogas and comparative studies can be made with available literature on premixed combustion of fossil fuels.
- The hydrogen-enrichment effects on premixed $C_3H_8/O_2/N_2$ and $C_3H_8/O_2/CO_2$ flames can be studied.
- Micromixer stabilized $C_3H_8/O_2/CO_2$ and $C_3H_8/O_2/N_2$ flames can be studied and compared with swirl stabilized ones.

# References:


[1] IEA. International Energy Outlook 2019.

[2] Seabra JEA, Macedo IC. Comparative analysis for power generation and ethanol production from sugarcane residual biomass in Brazil. Energy Policy 2011;39:421–8.

[3] Akay G, Jordan CA. Gasification of fuel cane bagasse in a downdraft gasifier: influence of lignocellulosic composition and fuel particle size on syngas composition and yield. Energy & Fuels 2011;25:2247–83.

[4] Li H, Yan J, Yan J, Anheden M. Impurity impacts on the purification process in oxyfuel combustion based CO2 capture and storage system. Applied Energy 2009;86 (2):202–13.

[5] Kang Y, Wei S, Zhang P, Lu X, Wang Q, Gou X, Huang X, Peng S, Yang D, Ji X. Energy 2017;119:1195–211.

[6] Zubairu Abubakar, Mohammad Raghib Shakeel, Esmail M.A. Mokheimer. Experimental and numerical analysis of non-premixed oxycombustion of hydrogen-enriched propane in a swirl stabilized combustor. Energy 2018;165:1401–14.

[7] Liu H, Zailani R, Gibbs BM. Comparisons of pulverized coal combustion in air and in mixtures of O2/CO2. Fuel 2005;84(7):833–40.

[8] Liu C Y, Chen G, Sipöcz N, Assadi M, Bai X S. Characteristics of oxy-fuel combustion in gas turbines. Applied Energy 2012;89(1):387–94.

[9] Oh J, Noh D, Lee E. The effect of CO addition on the flame behavior of a nonpremixed oxy-methane jet in a lab-scale furnace. Applied Energy 2013;112:350–7.

[10] Song Y, Zou C, He Y, Zheng C. The chemical mechanism of the effect of CO2 on the temperature in methane oxy-fuel combustion. International Journal of Heat and Mass Transfer 2015;86:622–8.

[11] Xie Y, Wang J, Zhang M, Gong J, Jin W, Huang Z. Experimental and numerical study on laminar flame characteristics of methane oxy-fuel mixtures highly diluted with CO2. Energy Fuels 2013, 27 (10), 6231−6237. Energy & Fuels 2013;27 (10):6231–7.

[12] Baukal CE. Oxygen-enhanced combustion. Boca Raton, USA: CRC Press LLC 1998.

[13] Gronkvist S, Bryngelsson M, Westermark M. Oxygen efficiency with regard to carbon capture. Energy 2006;31:3220–6.

[14] Mondal MK, Balsora HK, Varchney P. Progress and trends in CO2 capture/ separation technologies: a review. Energy 2012;46:431–41.

[15] Wall TF. Combustion processes for carbon capture. Proceedings of the Combustion Institute 2007;31(1):31–47.

[16] Nemitallah MA. A study of methane oxy-combustion characteristics inside a modified design button-cell membrane reactor utilizing a modified oxygen permeation model for reacting flows. Journal of Natural Gas Science and Engineering 2016;28:61–73.

[17] Nemitallah MA, Habib MA, Mezghani K. Experimental and numerical study of oxygen separation and oxy-combustion characteristics inside a button-cell LNO-ITM reactor. Energy 2015;84:600–11.

[18] Habib MA, Salaudeen SA, Nemitallah MA, Ben-Mansour R, Mokheimer EMA. Numerical investigation of syngas oxy-combustion inside a LSCF-6428 oxygen. transport membrane reactor. Energy 2016;96:654–65.

[19] Zhang J, Mi J, Li P, Wang F, Dally B. Moderate or intense low-oxygen dilution combustion of methane diluted by CO2 and N2. Energy & Fuels 2015;29(7):4576–85.

[20] Williams T C, Shaddix C R, Schefer R W. Effect of syngas composition and CO2-diluted oxygen on performance of a premixed swirl-stabilized combustor. Combustion Science and Technology 2007;180(1):64–88.

[21] Jourdaine P, Mirat C, Caudal J, Lo A, Schuller T A. Comparison between the stabilization of premixed swirling CO2- diluted methane oxy-flames and methane/air flames. Fuel 2017;201:156–64.

[22] Xie Y, Wang J, Zhang M, Gong J, Jin W, Huang Z. Experimental and numerical study on laminar flame characteristics of methane oxy-fuel mixtures highly diluted with CO2. Energy & Fuels 2013;27(10):6231–7.

[23] Kim H S, Arghode V K, Gupta A K. Flame characteristics of hydrogen-enriched methane-air premixed swirling flames. International Journal of Hydrogen Energy 2009;34(2):1063–73.

[24] SES6-502596, European Commission, European hydrogen roadmap: contract EUR-OP, Luxembourg. 2008.

[25] Wietschel M BM. The future of hydrogen opportunities and challenges. Economic Opportunities and Challenges 2009:613–39.

[26] Edwards P P, Kuznetsov V L, David W I F, Brandon N P. Hydrogen and fuel cells: Towards a sustainable energy future. Energy Policy 2008;36:4356–62.

[27] Pandey P, Pundir B P, Panigrahi P K. Hydrogen addition to acetylene-air laminar diffusion flames: Studies on soot formation under different flow arrangements.

Combustion and Flame 2007;148:249–62.

[28] Park SH, Lee KM, Hwang CH. Effects of hydrogen addition on soot formation and oxidation in laminar premixed C2H2/air flames. International Journal of Hydrogen Energy 2011;36:9304–11.

[29] Suliman Abdelwahid, Medhat Nemitallah, Binash Imteyaz, Ahmed Abdelhafez, Mohamed Habib. Effects of H2 Enrichment and Inlet Velocity on Stability Limits and Shape of CH4/H2−O2/CO2 Flames in a Premixed Swirl Combustor. Energy & Fuels 2018;32:9916–25.

[30] Shy S S, Chen Y C, Yang C H, Liu C C, Huang C M. Effects of H2 or CO2 addition, equivalence ratio, and turbulent straining on turbulent burning velocities for lean premixed methane combustion. Combustion and Flame 2008;153(4):510–24.

[31] Guo H, Smallwood G J, Liu F, Ju Y, Gülder Ö L. The effect of hydrogen addition on flammability limit and NOx emission in ultra-lean counterflow CH4/air premixed flames. Proceedings of the Combustion Institute 2005;30(1):303–10.

[32] Imteyaz B, Medhat A Nemitallah, Ahmed A Abdelhafez, Mohamed A Habib. Combustion behavior and stability map of hydrogen-enriched oxy-methane premixed flames in a model gas turbine combustor. International Journal of Hydrogen Energy 2018;43:16652–66.

[33] Boushaki T, Dhué Y, Selle L, Ferret B, Poinsot T. Effects of hydrogen and steam addition on laminar burning velocity of methane-air premixed flame: Experimental and numerical analysis. International Journal of Hydrogen Energy 2012;37:9412–22.

[34] F. Halter, C. Chauveau, I. Gökalp. Characterization of the effects of hydrogen addition in premixed methane/air flames. International Journal of Hydrogen Energy 2007;32:2585–92. doi:https://doi.org/10.1016/j.ijhydene.2006.11.033.

[35] Yu G, Law CK, Wu CK. Laminar flame speeds of hydrocarbon + air mixtures with hydrogen addition. Combustion and Flame 1986;63:339–47.

[36] Vagelopoulos CM, Egolfopoulos FN. Direct experimental determination of laminar flame speeds. Symposium (International) on Combustion 1998;27 (1):513–9.

[37] Galmiche B, Halter F, Foucher F, Dagaut P. Effects of dilution on laminar burning velocity of premixed methane/air flames. Energy & Fuels 2011;25 (3):948–54.

[38] Taamallah S, Chakroun NW, Watanabe H, Shanbhogue SJ, Ghoniem AF. On the characteristic flow and flame times for scaling oxy and air flame stabilization modes in premixed swirl combustion. Proceedings of the Combustion Institute 2017;36(3):3799–807.

[39] Wu KK, Chang YC, Chen CH, Chen YD. High-efficiency combustion of natural gas with 21-30% oxygen-enriched air. Fuel 2010;89:2455–62.

[40] Merlo N, Boushaki T, Chauveau Ch, Persis SD, Pillier L, Sarh B, Gokalp I. Combustion characteristics of methane-oxygen enhanced air turbulent non-premixed swirling flames. Experimental Thermal and Fluid Science 2013;56:53–60.

[41] Daood SS, Nimmo W, Edge P, Gibbs BM. Deep-staged, oxygen enriched combustion of coal. Fuel 2012;101:187–96.

[42] Tan Y, Douglas MA, Thambimuthu KV. CO2 capture using oxygen enhanced combustion strategies for natural gas power plants. Fuel 2002;81:1007–16.

[43] Horbaniuc B, Marin O, Domitras, Cu G, Charon O. Oxygen-enriched combustion in supercritical steam boilers. Energy 2004;29:427–48.

[44] Qiu K, Hayden ACS. Increasing the efficiency of radiant burners by using polymer membranes. Applied Energy 2009;86:349–54.

[45] Lambert J, Sorin M, Paris J. Analysis of oxygen-enriched combustion for steam methane reforming (SMR). Energy 1997; 22:817-25. Energy 1997;22:817–25.

[46] Kaskan WE. The dependence of flame temperature on mass burning velocity. Symposium Combustion 1957;6(1):134–43.

[47] Van Maaren A, Thung DS, De Goey LPH. Measurement of flame temperature and adiabatic burning velocity of methane/air mixtures. Combustion Science and Technology 1994;96(4-6):327–44.

[48] Liao SY, Jiang DM, Huang ZH, Zeng K, Cheng Q. Determination of the laminar burning velocities for mixtures of ethanol and air at elevated temperatures. Applied Thermal Engineering 2007;27(2-3):374–80.

[49] Metghalchi M, Keck JC. Laminar burning velocity of propane-air mixtures at high temperature and pressure. Combustion and Flame 1980;38:1443–54.

[50] Shroll AP, Shanbhogue SJ, Ghoniem AF. Dynamic-stability characteristics of premixed methane oxy-combustion. Journal of Engineering for Gas Turbines and Power 2012;134 (5).

[51] Kutne P, Kapadia BK, Meier W, Aigner M. Experimental analysis of the combustion behaviour of oxyfuel flames in a gas turbine model combustor. Proceedings of the Combustion Institute 2011;33:3383–90. doi:10.1016/j.proci.2010.07.008.

[52] Chu H, Yan Y, Xiang L, Han W, Ren F, Peng L. Effect of oxygen-rich combustion on soot formation in laminar co-flow propane diffusion flames. Journal of the Energy Institute 2019. doi:https://doi.org/10.1016/j.joei.2019.04.015.

[53] Zubairu Abubakar, Mohammad Raghib Shakeel, Esmail M.A. Mokheimer. Experimental and numerical analysis of non-premixed oxycombustion of hydrogen-enriched propane in a swirl stabilized combustor. Energy 2018;165:1401–14.

[54] Hu E, Huang Z, He J, Jin C, Zheng J. Experimental and numerical study on laminar

burning characteristics of premixed methane – hydrogen – air flames. International Journal of Hydrogen Energy 2009;34:4876–88.

[55] Di Sarli V, Di Benedetto A. Laminar burning velocity of hydrogen-methane/air premixed flames. International Journal of Hydrogen Energy 2007;32:637–46.

[56] Tang C, Huang Z, Jin C, He J, Wang J, Wang X, et al. Laminar burning velocities and combustion characteristics of propane-hydrogen-air premixed flames. International Journal of Hydrogen Energy 2008;33:4906–14.

[57] R Sankaran, Hong G IM. Effects of Hydrogen Addition on the Markstein Length and Flammability Limit of Stretched Methane/Air Premixed Flames. Combustion Science and Technology 2006;178:1585–611.

[58] Nakahara M, Kido H. Study on the Turbulent Burning Velocity of Hydrogen Mixtures Including Hydrocarbons. American Institute of Aeronautics and Astronautics 2008;46.

[59] Daniele S, Jansohn P, Boulouchos Konstantinos. Experimental Investigation of Lean Premixed Syngas Combustion at Gas Turbine Relevant Conditions. Italian Section of the Combustion Institute 2009.

[60] Daniele S, Jansohn P, Mantzaras J, Boulouchos K. Turbulent flame speed for syngas at gas turbine relevant conditions. Proceedings of the Combustion Institute 2011;33:2937–44.

[61] Liu F, Guo H, Smallwood G J. The chemical effect of CO2 replacement of N2 in air on the burning velocity of CH4 and H2 premixed flames. Combustion and Flame 2003;133:495–7.

[62] Schefer RW. Hydrogen enrichment for improved lean flame stability. International Journal of Hydrogen Energy 2003;28:1131–41.

[63] Cheng R K, Littlejohn D. Laboratory Study of Premixed H2-Air and H2–N2-Air Flames in a Low-Swirl Injector for Ultralow Emissions Gas Turbines. The Journal of Engineering for Gas Turbines and Power 2008;130(3).

[64] Ahmed Abdelhafez, Sherif S. Rashwan, Medhat A. Nemitallah, and Mohamed A. Habib. Stability map and shape of premixed CH4/O2/CO2 flames in a model gas-turbine combustor. Applied Energy 2018;215:63–74.

[65] Medhat A Nemitallah, Binash Imteyaz, Ahmed Abdelhafez, and Mohamed A Habib. Experimental and computational study on combustion and stability characteristics of CH4-H2-O2-CO2 premixed flames for gas turbine applications. Applied Energy 2019;250:433–43.

[66] Joshi ND, Epstein MJ, Durlak S, Marakovits S, Sabla PE. Development of a fuel air premixer for aero-derivative dry low emissions combustors. Interational Gas Turbine and Aeroengine Congress and Exposition 1994;94:1–9.

[67] Brohez S, Delvosalle C, Marlair G. A two-thermocouples probe for radiation corrections of measured temperatures in compartment fires. Fire Safety Journal 2004;39:399–411.

[68] Nemitallah MA, Habib MA. Experimental and numerical investigations of an atmospheric diffusion oxy-combustion flame in a gas turbine model combustor. Applied Energy 2013; 111: 401-15. Applied Energy 2013;111:401–15.

[69] Ahmed Abdelhafez, Sherif S. Rashwan, Medhat A. Nemitallah, Mohamed A. Habib. Stability map and shape of premixed CH4/O2/CO2 flames in a model Gas turbine Combustor. Applied Energy 2018;215:63–74.

[70] Carr NL, Kobayashi R, Burrows DB. Viscosity of hydrocarbon gases under pressure. Journal of Petroleum Technology 1954;6(10):47–55.

[71] Cengel YA, Boles MA. Thermodynamics an engineering approach 2015.

[72] Chen L, Ghoniem AF. Simulation of Oxy-Coal Combustion in a 100 kW th Test Facility Using RANS and LES: A Validation Study. Energy & Fuels 2012;26:4783–98.

[73] Porter R, Liu F, Pourkashanian M, Williams, Smith D. Evaluation of solution methods for radiative heat transfer in gaseous oxy-fuel combustion environments. Journal of Quantitative Spectroscopy and Radiative Transfer 2010;111:2084–94.

[74] Johansson R, Leckner B, Andersson K, Johnsson F. Account for variations in the H2O to CO2 molar ratio when modelling gaseous radiative heat transfer with the weighted-sumof- grey-gases model. Combustion and Flame 2011;158:893–901.

[75] Rajhi MA, Ben-Mansour R, Habib MA, Nemitallah MA, Andersson K. Evaluation of gas radiation models in CFD modeling of oxy-combustion. Energy Conversion and Management 2014;81:83–97.

[76] Ahmed Abdelhafez, Medhat A Nemitallah, Sherif S Rashwan, and Mohamed A Habib. Adiabatic Flame Temperature for Controlling the Macrostructures and Stabilization Modes of Premixed Methane Flames in a Model Gas-Turbine Combustor. Energy & Fuels 2018;32:7868–77.

[77] Jerzak W, Kuźnia M. Experimental study of impact of swirl number as well as oxygen and carbon dioxide content in natural gas combustion air on flame flashback and blow-off. Journal of Natural Gas Science and Engineering 2016;29:46–54.

[78] Habib M A, Rashwan S S, Nemitallah MA, Abdelhafez A. Stability maps of non-premixed methane flames in different oxidizing environments of a gas turbine model combustor. Appl Energy 2017;189:177–86. n.d. MA, Abdelhafez A. Stability maps of non-premixed met. Applied Energy 2017;189:177–86.

[79] Zhongqiu Li, Xiaobei Cheng, Wenming Wei, Liang Qiu, Hui Wu. Effects of hydrogen addition on laminar flame speeds of methane, ethane and propane: Experimental and numerical analysis. International Journal of Hydrogen Energy

2017;42:24055–66.

[80] C. L. Tang, Z. H. Huang CKL. Determination, correlation, and mechanistic interpretation of effects of hydrogen addition on laminar flame speeds of hydrocarbon–air mixtures. Proceedings of the Combustion Institute 2011;33:921–8.

[81] M A Nemitallah, G Kewlani, S Hong, S J Shanbhogue, M A Habib, A F Ghoniem. Investigation of a turbulent premixed combustion flame in a backward-facing step combustor; effect of equivalence ratio. Energy 2016;95:211–22.

# Vitae


| | | |
|---|---|---|
| Name | : | Asif Ali |
| Nationality | : | Pakistan |
| Date of Birth | : | 11-Oct-1993 |
| Email | : | asif_munawar_93@hotmail.com |
| Address | : | House 30, Block-A, Al-Madina Housing Society, Tandojam 70060 Hyderabad, Pakistan |


Publications:

1. Static Stability and Combustion Characteristics of Oxy-Propane Flames in a Premixed Fuel-Flexible Swirl Combustor, Energy & Fuels, DOI: 10.1021/acs.energyfuels.9b03157.
2. Frontiers in combustion techniques and burner designs for emissions control and CO2 capture: A review, International Journal of Energy Research, 2019, 1-33, DOI: 10.1002/er.4730.